

Higgs relaxation after inflation

Nayara Fonseca,^a Enrico Morgante,^a Géraldine Servant^{a,b}

^a DESY, Notkestrasse 85, 22607 Hamburg, Germany

^b II. Institute of Theoretical Physics, Univ. Hamburg, D-22761 Hamburg, Germany

Abstract. We show that the mechanism of cosmological relaxation of the electroweak scale can take place independently of the inflation mechanism, thus relieving burdens from the original relaxion proposal. What eventually stops the (fast-rolling) relaxion field during its cosmological evolution is the production of particles whose mass is controlled by the Higgs vacuum expectation value. We first show that Higgs particle production does not work for that purpose as the Higgs field does not track the minimum of its potential in the regime where Higgs particles get efficiently produced through their coupling to the relaxion. We then focus on gauge boson production. We provide a detailed analysis of the scanning and stopping mechanism and determine the parameter space for which the relaxion mechanism can take place after inflation, while being compatible with cosmological constraints, such as the relaxion overabundance and Big Bang Nucleosynthesis. We find that the cutoff scale can be as high as several hundreds of TeV. In this approach, the relaxion sector is responsible for reheating the visible sector. The stopping barriers of the periodic potential are large and Higgs-independent, facilitating model-building. As a result, the relaxion is quite heavy, from 0.1 GeV up to the cutoff. In this scenario, the relaxion field excursion is many orders of magnitude smaller than in the original relaxion proposal (subplanckian). We also discuss whether the relaxion may leave detectable signatures at future experiments.

Contents

1	Introduction	2
2	General conditions for relaxation after inflation	4
2.1	Relaxion in a non-inflationary phase and the reheating of the universe	5
2.2	Relaxion initial velocity	10
2.3	Higgs field following its minimum	12
2.4	Baryogenesis	13
3	General conditions for relaxation through particle production	14
3.1	Friction from Higgs particle production	14
3.2	Stopping the relaxion with gauge bosons production	15
4	Parameter space for successful relaxation of the EW scale through gauge bosons production	20
5	Relaxion properties	26
5.1	Relaxion mass and mixing with the Higgs	26
5.2	Relaxion lifetime	28
6	Cosmological constraints	29
6.1	Relaxion abundance in the early universe	30
6.1.1	Vacuum misalignment	30
6.1.2	Thermal production	31
6.2	Dark matter relic abundance	32
6.3	Primordial abundances of light elements	32
6.4	CMB distortions	32
6.5	Entropy injection before CMB formation	33
6.6	Reionization	33
6.7	Overview	34
7	Summary and Conclusions	36
A	Equations of Motion	38
A.1	Higgs case	38
A.2	Gauge bosons case	39

1 Introduction

Recently, a new mechanism has been proposed to generate a naturally small electroweak scale without relying on new symmetries at the electroweak scale [1]. It exploits the coupling of the Higgs boson to an axion-like field which induces a long cosmological evolution of the Higgs mass parameter. This is the so-called *relaxion mechanism*. While classically rolling down its potential, the relaxion field scans down the Higgs mass parameter, starting from a value of the order of the cutoff scale, until a stopping mechanism comes into play precisely when the Higgs mass parameter approaches zero. This would naturally explain the smallness of the Higgs mass parameter compared to the cutoff scale of the theory. In this context, there may be no expectation for the existence of new particles at the TeV scale. Instead, one predicts at least one very light and very weakly interacting particle.

This very change of paradigm has therefore far-reaching implications for strategies to search for new physics linked to the understanding of the weak scale and has consequently triggered a large literature: On general model building concerns [2–8], on attempts to do this without inflation [9, 10], on issues related to inflation [11–17] and reheating [18], on UV completions involving supersymmetry [15, 19, 20], composite Higgs [21–23], two-Higgs-doublet models [24], a mirror copy of the Standard Model [25], a Nelson-Barr model [26], clockwork axions [27–29], warped extra dimensions [30] or other constructions with multiple axions [31], on phenomenological aspects and experimental signatures [32–35], and on alternative implementations of the mechanism that do not require any barriers [36, 37].

In the original proposal [1] (GKR), the system starts in the symmetric electroweak phase and stopping barriers in the periodic relaxion potential with period f get generated only once the Higgs mass parameter turns tachyonic. Such mechanism relies on Higgs-dependent barriers as well as a long period of inflation to guarantee the slow classical evolution of the relaxion. The slope of the potential along which the axion-like field is rolling and its coupling to the Higgs field are generated due to a small effective breaking of a shift symmetry. This can be reconciled with the pseudo-Nambu-Goldstone (PNGB) boson nature of the relaxion if the slope arises from a second oscillatory potential with a period much larger than f in the so-called clockwork axion framework [27–29], in N -site constructions [31] or in warped extra-dimensional ones [30].¹

If the relaxion is the QCD axion (GKR1), the Peccei-Quinn solution to the strong CP problem can be preserved only if new dynamics is introduced at the end of inflation. Besides, the cutoff scale cannot be pushed higher than 30 TeV while the coupling between the Higgs and the relaxion has to be smaller than 10^{-30} (see [38, 39] for an updated discussion on this model). If instead the relaxion comes from a new strongly interacting sector (GKR2), the cutoff scale can be pushed up to 10^8 GeV. However, this

¹A completely different approach for a UV completion was discussed in string compactifications. It was shown in [8] that UV completions of the relaxion in string theory realizations via axion monodromy are strongly constrained. The field excursion corresponds to a physical charge carried by branes or fluxes which backreacts on the ten-dimensional configuration, and can suppress the barriers generated by strong gauge dynamics. This leads to a “runaway” relaxion, thus ruining the stopping mechanism.

requires new EW scale fermions, generating a coincidence problem. This problem was solved via a double-scanner mechanism in [2] where the barrier height depends on an additional extra field. In this context, initial conditions are very different from GKR1 and GKR2 as the barrier’s height starts large until it gets cancelled by the additional scanner field. Overall, the maximal cutoff scale that can be achieved by the relaxion mechanism is $\sim 10^8$ GeV. At this scale, it is assumed that some other mechanism kicks in to protect the Higgs mass against the Planck scale, either via supersymmetry, compositeness, or other mechanisms.

A successful implementation of the original relaxion proposal requires a low scale of inflation associated with non-trivial inflation model building. This has tarnished the appeal of the relaxion mechanism. We are therefore interested to consider instead the possibility that the friction acting on the relaxion is not provided by an inflation era but instead by particle production during the field classical evolution. This would enable to decouple the relaxion mechanism from inflation and thus no further constraint on the number of e-folds or inflation scale would be imposed. A very interesting framework along these lines was proposed in [10], where the source of particle production comes from a single higher-dimensional coupling between the relaxion and a $U(1)$ gauge field. A motivation of the authors was to avoid superplanckian field excursions (see also [40, 41]). While the conditions for a successful friction mechanism were derived, a full derivation of all phenomenological constraints and a precise picture of the cosmological history in this context was lacking. This is what we do in this work. In addition, we show explicitly why the relaxion coupling to the Higgs cannot lead to a friction term from Higgs particle production. Relying on the relaxion coupling to a combination of SM gauge fields, we suggest that the relaxion may be responsible for the reheating of the universe, thus connecting reheating and the Higgs sector. We also stress that the relaxion is much heavier than in the original GKR proposal and can be much larger than the GeV scale. In Ref. [10], the impact of particle production on the relaxion mechanism was discussed before inflation, during inflation and at the end of inflation. In our setup, we focus on the situation where one can ignore the inflaton. The relaxion is dominating the energy density of the universe during relaxation, although it is not slow-rolling.

In this setup, the main improvements compared to the ‘standard relaxion’ models are:

- a weak scale relaxation mechanism independent from inflation (no need for a gigantic number of e-folds \mathcal{N}_e nor a small Hubble rate during inflation H_I);
- sub-Planckian field excursions for the relaxion;
- the barriers of the relaxion periodic potential are independent from the Higgs vacuum expectation value;

The plan of the paper is the following. In Section 2, we discuss the general conditions for realizing the relaxion mechanism after inflation. In Section 3, we discuss the conditions for using particle production as friction instead of inflation. We consider first Higgs particle production and then gauge boson production. The relaxion

properties are presented in Section 5. We then consider in Section 6 all phenomenological and cosmological constraints (relic abundance, Big Bang nucleosynthesis (BBN), cosmic microwave background (CMB), and reionization) and determine the parameter space where a successful implementation is realised. We conclude in Section 7. The equations of motion for the Higgs, relaxion and the gauge bosons are reproduced in Appendix A, with a display of their numerical solutions.

2 General conditions for relaxation after inflation

The scalar potential for the Higgs h and relaxion ϕ fields reads:

$$V(\phi, h) = \Lambda^4 - g\Lambda^3\phi + \frac{1}{2}(-\Lambda^2 + g'\Lambda\phi)h^2 + \frac{\lambda}{4}h^4 + \Lambda_b^4 \cos\left(\frac{\phi}{f'}\right), \quad (2.1)$$

where Λ is the cutoff scale up to which we want to solve the hierarchy problem using the relaxion. The relaxion ϕ is an axion-like field with decay constant f' . The dimensionless couplings g and g' are assumed to be spurions that quantify the explicit breaking of the axion shift symmetry, and Λ_b is the scale at which the ϕ periodic potential is generated. The term Λ^4 cancels the final value of the cosmological constant and corresponds to the usual tuning of the cosmological constant.

We want the scanning of the Higgs mass parameter to occur when the inflaton is a subdominant component of the energy of the universe so as to decouple the relaxation scenario from inflation. For that, a crucial difference with respect to the the original relaxion scenario [1] is that we start in the broken electroweak phase, where the Higgs mass parameter in the Higgs potential is large and negative [10]. Another important difference is that that the amplitude Λ_b^4 of the cosine potential is constant and does not depend on the Higgs vacuum expectation value.² We require $g \gtrsim g'/(16\pi^2)$ for the stability of the potential (closing the Higgs loop from the third term in Eq. (2.1) generates the slope $\sim g\Lambda^3\phi$). In our numerical analysis, we will take $g = g'$.

The cosmological history is the following. After inflation ends, the universe is reheated. As soon as the temperature drops below $\sim \Lambda$, the shift symmetry that protects the relaxion potential breaks and ϕ starts rolling. The scanning of the Higgs mass parameter starts. The initial condition for ϕ is such that the Higgs field has a large negative mass term, which corresponds to

$$-\mu_h^2 \equiv -\Lambda^2 + g'\Lambda\phi \ll 0. \quad (2.2)$$

The electroweak symmetry is broken and all gauge bosons coupled to the Higgs have large masses. The friction is negligible and the relaxion rolls down its potential with some high speed, overshooting the large barriers. The Higgs mass parameter is thus scanned as the vacuum expectation value (VEV) of the relaxion is increasing. The relaxion evolves towards large positive values until it approaches the critical point $\phi_c \equiv \Lambda/g'$ where the Higgs mass term is zero. As the electroweak gauge bosons

²The existence of large barriers was also present in the double scanning mechanism of the CHAIN model presented in [2].

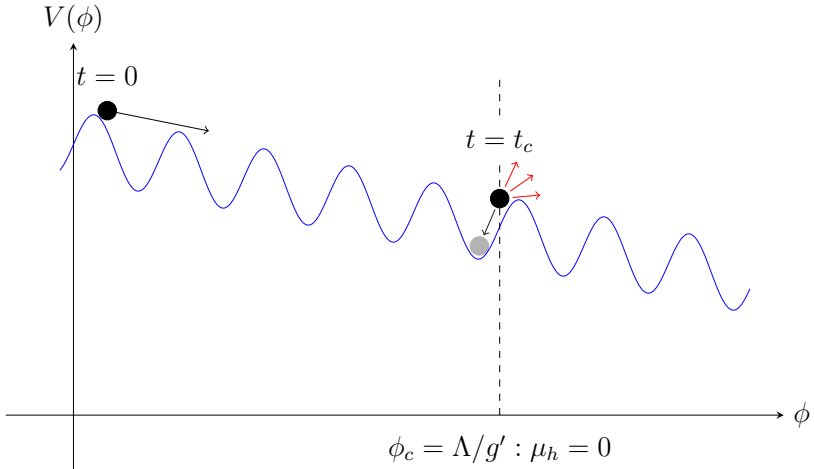
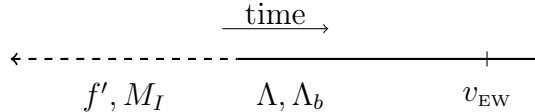


Figure 1. Sketch of the relaxion field evolution.

become light enough, they can be produced exponentially through their coupling to the relaxion. As we will discuss in Sec. 3, this particle production is so efficient that it quickly slows down the relaxion, which has no longer enough kinetic energy to overshoot the barriers. The relaxion is therefore stopped right before it reaches the critical point ϕ_c , in such a way that the final Higgs VEV is small compared to its initial value set by Λ . The use of particle production in relaxion models appeared previously in [10] (see also [18, 37, 40]).

In the sketch below we show the hierarchy of scales $(f', M_I > \Lambda, \Lambda_b > v_{\text{EW}})$, where the solid line indicates when the scanning starts and M_I is the inflation scale.



A sketch of the relaxion potential and its evolution is shown in Fig. 1.

2.1 Relaxation in a non-inflationary phase and the reheating of the universe

To realize the relaxation mechanism after the end of inflation, it is crucial to discuss how the temperature affects the scenario described above. As we shall see in the following, there are two possibilities for the reheating: (i) the inflaton sector reheats the SM degrees of freedom, and (ii) the inflaton reheats a hidden sector decoupled from the SM and later the relaxion reheats the visible sector. In what follows we will discuss these two possibilities, and we will show that the first case can be realized only in the region of the parameter space corresponding to the smallest values of the coupling g' .

First, let us assume that, at the end of the inflationary phase, the energy density of the inflaton field is transferred to the SM sector, initiating the radiation era. Relaxation starts when the temperature drops below the cutoff Λ of the theory and the potential

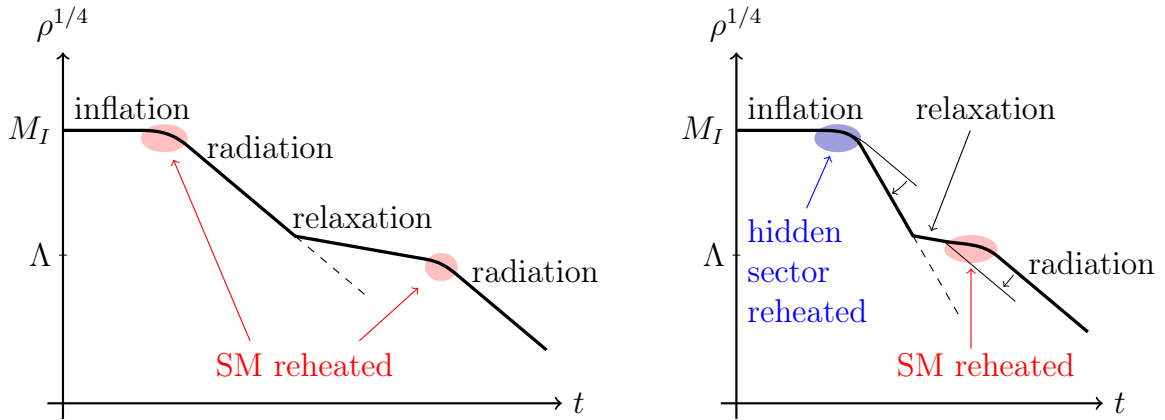


Figure 2. Sketch of the evolution of the energy density of the universe under two distinct assumptions about the first reheating stage. *Left:* The inflaton reheats the visible sector, and relaxation starts when its temperature drops below Λ . The period of relaxation is characterised by a short stage of inflation lasting for a few e-folds as needed to suppress the thermal mass of the Higgs. A second reheating takes place after relaxation. *Right:* The inflaton transfers its energy to a hidden sector, and the visible one is reheated after relaxation. In this case, the relaxation phase can be short, and some mechanism to dilute the dark radiation is needed. For example, a period of kinetic energy domination in the dark sector or a prolonged reheating phase with a matter-like equation of state can be sufficient to suppress the dark component with respect to the visible one.

$V(\phi)$ is generated. The relaxion then dominates the energy density until it is stopped and its energy is converted into radiation. A sketch of how the energy density evolves is shown in the left panel of Fig. 2. During the relaxation era, the equation of state changes along the evolution, with $w = p/\rho < 0$ and close to $w = -1$ (cosmological constant) for the lowest values of the coupling g' .

An important concern comes from the fact that, if the SM is reheated to a too high temperature, the negative mass-squared of the Higgs field is turned positive by a thermal mass term $\sim y_t^2 T^2$. This could spoil the relaxation mechanism, since the field ϕ would stop in the wrong position as soon as $\mu_h^2 + y_t^2 T^2 = 0$, where $y_t \sim 1$ is the top Yukawa. To consider this issue more carefully, we have to compare the time scales of relaxation with that of the cooling of the universe. Relaxation starts when the temperature drops below $T \sim \Lambda$. Initially, the squared mass term μ_h^2 and the Higgs thermal mass are both of order Λ , and we have to assume that the former is larger than the latter. As relaxation goes on, both terms will decrease. In order for the mechanism not to be spoiled by thermal effects, it is necessary that the condition

$$|\mu_h| \gtrsim T \quad (2.3)$$

holds during the whole process. The validity of condition (2.3) in terms of the parameters Λ and g' can be understood as follows. The temperature at the end of relaxation

must be smaller than the electroweak scale $T_{\text{end}} \lesssim v_{\text{EW}}$ and $T_{\text{ini}} \sim \Lambda$, then we have

$$\frac{a_{\text{ini}}}{a_{\text{end}}} \lesssim \frac{v_{\text{EW}}}{\Lambda}, \quad (2.4)$$

where $a_{\text{ini}} \equiv a(t = t_{\text{ini}})$ and $a_{\text{end}} \equiv a(t = t_{\text{end}})$ and we used that the temperature scales with the inverse of the scale factor. On the other hand, $a_{\text{ini}}/a_{\text{end}} = \exp(-\int H dt) \equiv e^{-\mathcal{N}}$, within \mathcal{N} being the number of e-folds, therefore condition (2.4) gives

$$\mathcal{N} \gtrsim \log\left(\frac{\Lambda}{v_{\text{EW}}}\right), \quad (2.5)$$

implying that the roll-down phase must last for at least a few e-folds. In the approximation of a constant Hubble rate $H \sim \Lambda^2/(\sqrt{3}M_{\text{Pl}})$ we get

$$\mathcal{N} \sim H\Delta t_{\text{rel}} \sim \frac{\Lambda}{\sqrt{3}g'M_{\text{Pl}}} \gtrsim \log\left(\frac{\Lambda}{v_{\text{EW}}}\right), \quad (2.6)$$

where we used that

$$\Delta t_{\text{rel}} \sim \frac{\Delta\phi}{\dot{\phi}} = \frac{\Lambda/g'}{\Lambda^2} = \frac{1}{g'\Lambda}, \quad (2.7)$$

which is obtained in the approximation of negligible Hubble friction. Additionally, the number of e-folds cannot be too large, in order not to wash out the perturbations generated during inflation, and therefore we impose that $\mathcal{N} \lesssim 20$.³ In this way one gets

$$\frac{\Lambda}{20\sqrt{3}M_{\text{Pl}}} \lesssim g' \lesssim \frac{\Lambda}{\sqrt{3}M_{\text{Pl}} \log(\Lambda/v_{\text{EW}})}, \quad (2.8)$$

leaving only a small window of parameter space open (imposing a more stringent bound on the duration of a secondary inflationary stage will reduce the region accordingly).

To check the validity of this naive estimate, we solved numerically the equation of motion for the relaxion field rolling down the linear potential, in an universe where the energy is initially equipartitioned between ϕ and radiation. The top panel of Fig. 3 shows the bounds in Eq. (2.8) and the comparison with the corresponding bounds computed numerically by solving the equations of motion. The difference in the two estimates is due to the assumption of constant Hubble rate in the analytical one. The other two lower panels show the evolution of the relaxion and radiation component of the energy density, and their contribution to Higgs mass parameter, for a benchmark point at $\Lambda = 10^4 \text{ GeV}$ and $g' = 10^{-15}$, that corresponds to a relaxation that lasts for ~ 10 e-folds. We see that the energy density is dominated by the relaxion, and that the thermal mass term is always subdominant with respect to the relaxion one, thus not spoiling the mechanism.

The bottomline of this discussion is that, if the SM is reheated to a temperature larger than the electroweak scale, there is little room for the relaxion mechanism to

³If the relaxion drives a long period of inflation, it is difficult to match the curvature perturbations that are generated in this phase with the COBE normalization [17].

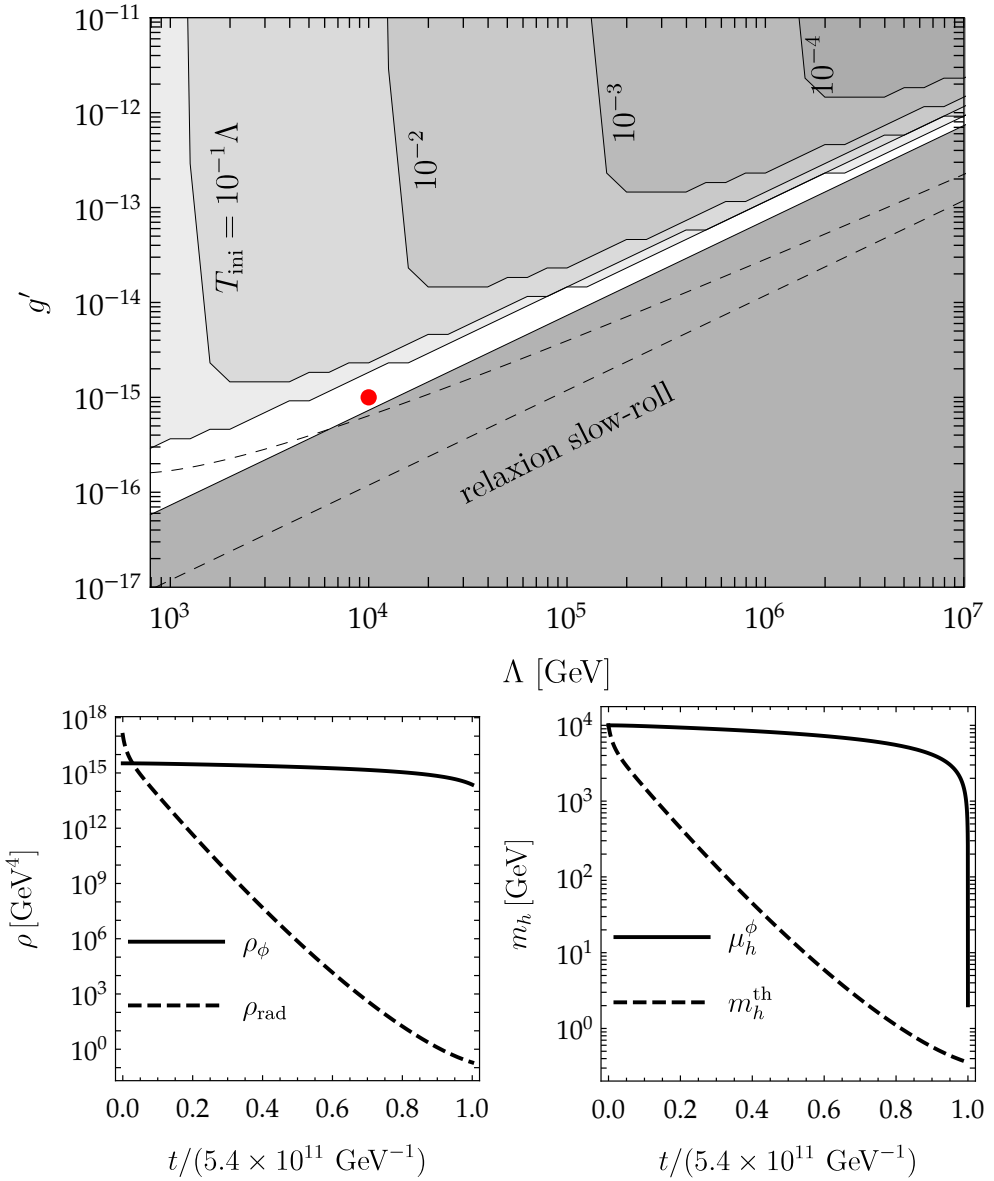


Figure 3. *Top:* In the white region, the temperature T of the visible universe (SM) is suppressed with respect to the EW scale and the relaxation lasts less than 20 e-folds. It is obtained by solving numerically the relaxion equation of motion in a universe where the energy is initially equipartitioned between the relaxion and radiation, and the initial temperature is $T_{\text{ini}} = \Lambda$. The dashed lines indicate the corresponding region obtained using the approximation Eq. (2.8). The different shades of gray show how the parameter space opens up if T_{ini} is assumed to be a fraction $10^{-1}, 10^{-2}, 10^{-3}, 10^{-4}$ of the cutoff scale Λ . *Bottom left:* Time evolutions of the relaxion energy density and radiation energy density for the benchmark point $\Lambda = 10^4 \text{ GeV}$, $g' = 10^{-15}$, marked in red in the top panel. *Bottom right:* Time evolutions of the Higgs mass term and the Higgs thermal mass for the same benchmark point.

take place after reheating, in the radiation era. If instead the reheating temperature of the universe is below the electroweak scale, the scanning can be finished during the radiation era without spoiling the mechanism. However, since the scale of inflation is larger than Λ , the relaxation process would start during the last e-folds of inflation or during the reheating phase. In this case, either relaxation takes place when the universe is still inflaton dominated [10], and the reheating phase has not yet started, or one has to worry about the maximal temperature of the SM plasma during reheating, which can exceed the EW scale.

On the other hand, one can assume that a large fraction of the energy which is initially stored in the inflaton field is transferred to a hidden sector gas, with no interaction with the SM, and that the temperature of the SM is much smaller than Λ at the time when relaxation starts. In this case, we can consider that the relaxion mechanism starts while the universe is in a radiation-dominated era and the temperature of the visible sector T is much smaller than the temperature of the universe, so that the bound presented in Eq. (2.6) is evaded for $T_{\text{ini}} \lesssim |\mu_h|$.⁴ The different shadings in the first panel of Fig. 3 show how the parameter space opens up if the temperature of the SM plasma at the beginning of the relaxation phase is taken to be a fraction $10^{-1}, 10^{-2}, 10^{-3}, 10^{-4}$ of the cutoff Λ .

In the following, we are going to assume for simplicity that the SM temperature after reheating is negligible, and all the energy is transferred to a sector decoupled from the SM. This implies that the upper bound on g' in Eq. (2.8) disappears and in the following we are simply going to assume the lower bound

$$g' \gtrsim 0.2 \frac{\Lambda}{M_{\text{Pl}}}, \quad (2.9)$$

which results from the numerical solution. Note that in this case Eq. (2.5) does not apply, and therefore the energy stored in the dark sector is not diluted during relaxation. In principle, this could be at odds with bounds on dark radiation. In order to avoid this, one can invoke for example a period of matter domination in the visible sector during the reheating phase or a period of kination domination in the hidden sector. This can efficiently dilute away the dark radiation (see right panel of Fig. 2). Another possibility is to assume that the hidden sector decays into the SM model after the reheating phase and before the BBN epoch.

In this scenario the role of particle production is two-fold: It stops the relaxion evolution at the right place and it reheats the visible sector after relaxation. In addition, ϕ can be responsible for the generation of the primordial curvature perturbations. If the Hubble rate H_I 60 e-folds before the end of inflation is larger than the scale Λ , then the field ϕ has to be regarded as a free field, which has quantum fluctuations governed by H_I . Then, the relaxion acts as a curvaton field, generating a sufficient amount of curvature perturbation, that is transferred to the SM during the particle production

⁴The same could be obtained if the reheating temperature is larger than v_{EW} , but a second field locks the relaxion at its initial position until the temperature has dropped, with a mechanism similar to [2, 30, 37]. While one can envisage a model of this kind, we are not going to discuss this possibility further.

phase. A detailed study of this aspect requires a dedicated study that we leave for future work.

2.2 Relaxion initial velocity

The initial velocity of the relaxion has to be large enough to overcome the barriers in the periodic potential. One could think that an initially small velocity is allowed for a generic initial position of ϕ , if the height of the barriers is small enough compared with the average slope of the potential, as it is shown Fig. 4. In the following we estimate under which condition the assumption of large initial velocity is not necessary, meaning that the field is in an ‘easy rolling’ regime. If the field starts rolling from a generic point ϕ_0 , that without loss of generality we assume to be in the interval $0 - 2\pi f'$, it will be able to overcome the first barrier at $2\pi f'$ and consequently start the rolling phase only if $V(\phi_0) > V(2\pi f')$. To quantify the requirement that this condition is generic, we impose that it holds for all values of ϕ_0 between 0 and $\pi f'$, implying $V(\pi f') \geq V(2\pi f')$, where

$$V(\pi f') = -g \Lambda^3 \pi f' + \Lambda_b^4 \cos\left(\frac{\pi f'}{f'}\right) \quad (2.10)$$

$$V(2\pi f') = -g \Lambda^3 2\pi f' + \Lambda_b^4 \cos\left(\frac{2\pi f'}{f'}\right) \quad (2.11)$$

In order for the relaxion to roll down easily, one obtains

$$\Lambda_b^4 \lesssim \pi g \Lambda^3 f'. \quad (2.12)$$

However, once particle production friction slows down the field, the constant periodic potential needs to cancel the slope, stopping the field evolution, which implies that the height of the barrier should be at least

$$\Lambda_b^4 \gtrsim g \Lambda^3 f'. \quad (2.13)$$

Therefore, in order to avoid an initial large velocity, one could in principle saturate this bound by assuming a coincidence of scales $\Lambda_b^4 \sim g \Lambda^3 f'$. Yet, at the end of the scanning process, the relaxion acquires a speed Λ^2 from the slope, and since ϕ has to be able to pass the barriers we have $\Lambda_b \lesssim \Lambda$, that would imply $\Lambda \sim g f'$. Unfortunately, this is in conflict with the condition on the precision of the Higgs mass scanning that we will discuss in Sec. 3, which requires Eq.(4.18), and which would imply $\Lambda^2 \lesssim m_h^2/(2\pi)$. We therefore disagree with the statement in [10, 41] that the relaxion can start at rest by assuming a coincidence of scales $\Lambda_b^4 \sim g \Lambda^3 f'$.

As a result, we have to assume that the initial velocity satisfies

$$\dot{\phi} \gtrsim \Lambda_b^2. \quad (2.14)$$

Realizing such a velocity as an outcome of a previous inflationary period is relatively simple. For example, one can introduce a coupling of the relaxion to the inflaton field, suppressed by a small coupling \tilde{g} , such that during inflation the relaxion obtains

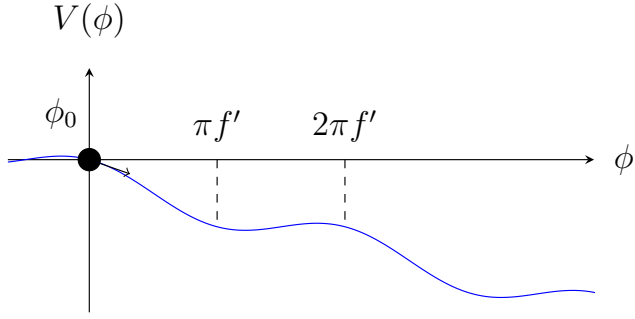


Figure 4. Sketch of the relaxion potential assuming a coincidence of scales that may avoid the requirement of initial large velocity. Here for convenience we set $V(\phi_0) = 0$ and $\phi_0 = 0$.

an effective slope $-\tilde{g}M_I^3\phi$. Then imposing that the slow-roll velocity of the relaxion is larger than Λ_b^2 we obtain $\tilde{g} \gtrsim \Lambda_b^2/(M_I M_{\text{Pl}})$, which would allow for a rather high inflationary scale while having a small coupling \tilde{g} . The smallness of the coupling \tilde{g} is important to guarantee that the shift symmetry is only softly broken, and in addition to avoid the reheating of the SM after inflation.⁵ Furthermore, a precise statement about the initial velocity requires to know the relaxion interaction with the hidden sector and also the UV physics that generate these barriers and how fast they appear. From now, we will assume Eq. (2.14).

A potential worry is if this velocity can be sustained during the relaxation phase, or whether the Hubble friction generated by the relaxion itself could reduce this velocity, in particular since the relaxion has to pass a very large number of barriers. We estimate the condition for this not to happen in the following way. Let us consider only the first barrier of the potential. The effect of Hubble friction is very small and we can use the approximate energy conservation to compute the velocity gain when the field goes from the first to the second peak. This has to be compared with the velocity loss due to Hubble friction, which is obtained as $\Delta\dot{\phi}_H = \int 3H\dot{\phi}dt \approx 6\pi f H$. Imposing that the first is larger than the second, one obtains

$$f' < \frac{g\Lambda^3}{9\pi H^2} - \frac{\dot{\phi}}{3\pi H} \approx \frac{gM_{\text{Pl}}^2}{9\pi\Lambda}, \quad (2.15)$$

where the second term was neglected in the last step and to get the last equality we used $\dot{\phi} \approx \Lambda^2$ and $H \approx \Lambda^2/M_{\text{Pl}}$. Given Eq. (2.9), condition (2.15) is trivially satisfied for sub-Planckian values of f' , which as we are going to see in Sec. 4 is always the case in our setup.

⁵ Assuming a coupling $\tilde{g}M_I^2\sigma\phi$, where σ is the inflaton, we estimate the decay width of the inflaton into SM fields through the mixing with the relaxion as $\Gamma \sim \tilde{g}^2 M_I^3/f^2$, where f is the scale controlling the coupling of the relaxion to gauge bosons that will be introduced in Sec. 3.2. To avoid reheating the SM one needs $\Gamma/H < 1$, which can be obtained by taking a small coupling \tilde{g} , while still satisfying the inequality above.

2.3 Higgs field following its minimum

In the case where the relaxation mechanism starts in the broken EW phase, we have to make sure that the Higgs field follows the minimum of its potential, to guarantee that the stopping mechanism is triggered when the Higgs VEV is small. Considering the potential in Eq. (2.1), the Higgs field has a minimum given by

$$v = \frac{1}{\sqrt{\lambda}}(\Lambda^2 - g'\Lambda\phi)^{1/2}. \quad (2.16)$$

If the Higgs field does not efficiently track the minimum of the potential, *i.e.* if it has a much larger value than the small value at the potential minimum near the critical value $(\Lambda^2 - g'\Lambda\phi_c) \approx 0$, then the relaxion mechanism is spoiled.

The Higgs efficiently follows the minimum of its potential as the mass is being scanned if the VEV evolves adiabatically, *i.e.*

$$\frac{\dot{v}}{v^2} \lesssim 1. \quad (2.17)$$

Note that $m_h^2 = 2\lambda v^2$ is the Higgs mass-squared. Therefore, assuming that the evolution starts with the Higgs field at the minimum, the relation (2.17) tells us that if the mass is large, the field is kept at the minimum of the correspondingly deep well in the potential during the scanning process. In the regime where the Higgs follows its minimum, we can write Eq. (2.17) in terms of the Higgs field,

$$h \gtrsim \frac{1}{\sqrt{\lambda}}(g'\Lambda\dot{\phi})^{1/3}, \quad (2.18)$$

where we assumed constant velocity $\dot{\phi}$. The success of the mechanism requires that Eq. (2.18) can only be violated when the Higgs field value is below the electroweak scale, then we impose

$$h \sim \frac{1}{\sqrt{\lambda}}(g'\Lambda\dot{\phi})^{1/3} \lesssim v_{\text{EW}}, \quad (2.19)$$

At the end of the evolution, the velocity is expected to be

$$\dot{\phi} \sim \mathcal{O}(\Lambda^2), \quad (2.20)$$

so the bound in Eq. (2.19) shows that we can make the Higgs follow the minimum of the potential as close as we want by decreasing g' and/or decreasing the cutoff scale Λ . As we shall see in Sec. 4, this is an important constraint in our parameter space. One can obtain the same result given in Eq. (2.19) by studying how efficiently the field tracks the minimum using the expansion of the Higgs around the tracking solution as in Ref. [10]. In Fig. 5, we compare the actual evolution of h and v with the approximation given by Eq. (2.19). These solutions were obtained by solving numerically the classical equations of motion for the fields. In the plots on the top, the Higgs does not track the minimum close enough to the critical point. In the plots on the bottom, the Higgs is efficiently following its minimum (the corresponding parameter values indicated in the caption are included in the scenario B in Sec. 3.2).

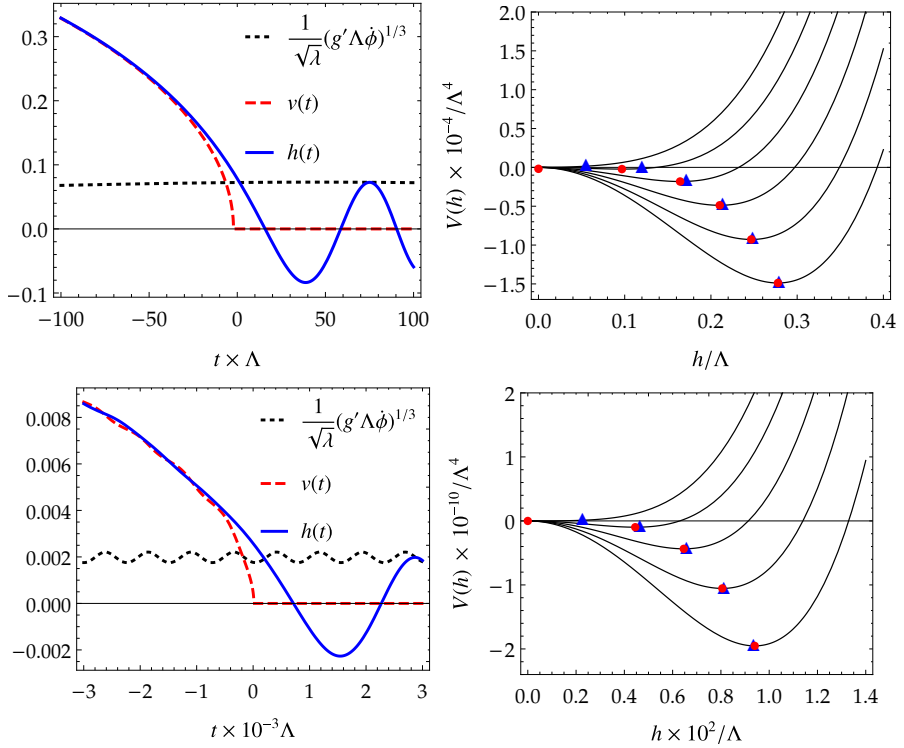


Figure 5. *Left:* Higgs field $h(t)$ (blue) and its value at the minimum of the potential $v(t)$ (red) as a function of time t in units of Λ^{-1} . The black curve indicates when the tracking stops from the approximation in (2.19) *Right:* Higgs potential where the blue points represent the field value and the red ones the value at the minimum. $\Lambda = 10^4$ GeV, $f' = 10^6$ GeV and $\Lambda_b = 7 \times 10^3$ GeV. *Top:* $g' = 10^{-4}$, the Higgs is not efficiently tracking the minimum of its potential (the tracking stops when the value at the minimum is still too large, $v \sim 0.1 \Lambda$). *Bottom:* $g' = 3 \times 10^{-9}$, the Higgs is efficiently following its minimum (the tracking stops when the value at the minimum is already below the electroweak scale, $v \sim 0.003 \Lambda$).

2.4 Baryogenesis

While we are interested to decouple the relaxion mechanism from inflation, it is important to note at this point that according to Fig. 2, while relaxation will happen after the reheating stage in which the inflaton energy density is transferred to an invisible sector, the relaxion energy density eventually takes over and a second reheating stage will follow at the end of relaxation when the energy density of the relaxion is transferred to the SM. The entropy injected in the plasma will then dilute the baryon asymmetry produced in earlier phases with a factor $(v_{\text{EW}}/\Lambda)^3$. This affects in particular a possible scenario in which baryogenesis takes place at high temperature before relaxation and with a very large Higgs VEV. Our relaxion mechanism therefore calls for some alternative baryogenesis mechanism taking place at the end of or after the relaxion mechanism. Electroweak baryogenesis is not option given that a first-order electroweak phase transition requires new physics at the electroweak scale, which is at odds with the relaxion principle. Other mechanisms will rely on non-vanishing $B - L$ processes. It might also be possible that the relaxion itself generates the baryon asym-

metry through the $\phi F\tilde{F}$ coupling with a mechanism similar to [42, 43]. As this work is being completed, a recent proposal appeared in [41] that is constrained by the bounds we derive in the following sections.

3 General conditions for relaxation through particle production

Particle production was successfully used to trap moduli fields at enhanced symmetry points [44] or to generate slow-roll inflation with a non-flat potential [45–47]. This mechanism was applied to the relaxion scenario in [10], exploiting the higher-dimensional anomalous coupling of the relaxion to a $U(1)$ linear combination of electroweak gauge fields. Here we will discuss this possibility in detail.

Before doing so, we start in the next subsection by considering the much more minimal possibility of Higgs particle production. This would be very appealing as it would not require any additional ingredient, exploiting the already existing Higgs-relaxion coupling. Unfortunately, it will turn out that there is a fundamental obstruction related to the requirement that the Higgs tracks the minimum of its potential. We will then turn our attention to the model in which the relaxion couples to the Chern-Simons term of the SM massive gauge bosons, as considered in [10] and derive the constraints that this mechanism poses on the parameter space. In Sec. 6, we will discuss the further cosmological bounds on this model.

3.1 Friction from Higgs particle production

Let us consider the case of production of Higgs particles through the coupling to the relaxion. We decompose the Higgs field h in a classical background field and a quantum fluctuation,

$$h = h_0 + \chi . \quad (3.1)$$

The set of equations of motion for the model in (2.1) can be found in App. A.1. One can study how a single Fourier mode $\chi_{\vec{k}}$ evolves by looking at the linearized equation of motion,

$$(\partial^2 + k^2 + g'\Lambda\phi - \Lambda^2 + 3\lambda h_0^2) \chi_{\vec{k}} = 0 . \quad (3.2)$$

Efficient particle production requires the adiabatic condition to be violated, *i.e.*

$$\left| \frac{\dot{\omega}_k}{\omega_k^2} \right| \gg 1 , \quad (3.3)$$

where

$$\omega_k = \sqrt{k^2 + (g'\phi\Lambda - \Lambda^2 + 3\lambda h_0^2)} \quad (3.4)$$

is the frequency of the quantum field $\chi_{\vec{k}}$. If one naively assumes that the field h_0 always efficiently tracks its minimum, Eq. (3.3) tells us that, for low momentum k , particle creation is efficient when $(g'\Lambda\phi_c - \Lambda^2) \approx 0$. This implies that $v \approx 0 \leftrightarrow \omega_k \approx 0$, where v is the Higgs minimum in Eq. (2.16). This behaviour would be exactly what we are looking for, meaning that particle production friction is large for small v , then

the relaxion could get trapped when the Higgs mass is small. More concretely, for low momentum k , Eq. (3.3) is satisfied if

$$\dot{\phi} \gtrsim 2\sqrt{2}(g'\Lambda)^{1/2} \left| \phi - \frac{\Lambda}{g'} \right|^{3/2}. \quad (3.5)$$

On the other hand, from Eq. (2.18), we know that the condition for the Higgs field to track the minimum of its potential is $h_0 \gtrsim (g'\Lambda\dot{\phi})^{1/3}/\sqrt{\lambda}$, leading to

$$\dot{\phi} \lesssim (g'\Lambda)^{1/2} \left| \phi - \frac{\Lambda}{g'} \right|^{3/2}. \quad (3.6)$$

Therefore, in the regime the approximations we use are valid, conditions (3.5) and (3.6) show that one cannot simultaneously have efficient particle production and the Higgs field following the minimum of its potential. This result may be expected as for the potential in Eq. (2.1) the condition (2.17) is basically the opposite of (3.3). In fact, for the benchmark points in Fig. 5, we find that the maximum of $|\dot{\omega}_k/\omega_k^2|$ are $|\dot{\omega}_k/\omega_k^2|_{\max} \sim 0.6$ and $|\dot{\omega}_k/\omega_k^2|_{\max} \sim 0.2$, respectively for the top and bottom cases in Fig. 5, showing that the adiabaticity condition is not violated in those cases.

3.2 Stopping the relaxion with gauge bosons production

We are now going to discuss the possibility that the relaxion is coupled to a massive vector field that becomes tachyonic when the VEV of the Higgs is sufficiently small. When the tachyonic instability occurs, the field grows exponentially, at the expense of the kinetic energy of the relaxion field, which decreases until the point $\dot{\phi} \sim \dot{\phi}_{\text{stop}} \lesssim \Lambda_b^2$ when the relaxion is no more able to overcome the barriers. Here we review the main ingredients and the constraints that we must impose for the successful implementation of the mechanism.

Given a generic vector field V_μ , its equation of motion presents a tachyonic instability if the field is coupled to the relaxion via a term

$$\frac{\phi}{4f} F_{\mu\nu} \tilde{F}^{\mu\nu}, \quad (3.7)$$

where $\tilde{F}^{\mu\nu} = \epsilon^{\mu\nu\rho\sigma} F_{\rho\sigma}$ (notice that this differs from the usual convention by a factor of 1/2). In our case, the field V_μ should be a massive SM vector, as we want its mass to be related to the Higgs VEV. It is crucial that the Lagrangian does not contain a term similar to Eq. (3.7) for the photon, as otherwise the tachyonic instability would be present during all the evolution, independently of the smallness of the Higgs mass. One can write the following Lagrangian, invariant under $\text{SU}(2) \times \text{U}(1)$ [10]:

$$\begin{aligned} \mathcal{L} = & \frac{1}{2} \partial_\mu \phi \partial^\mu \phi + (\mathcal{D}_\mu \Phi_H)^\dagger \mathcal{D}^\mu \Phi_H - \frac{1}{2} \text{Tr}[W_{\mu\nu} W^{\mu\nu}] - \frac{1}{4} B_{\mu\nu} B^{\mu\nu} \\ & - \frac{\phi}{4f} \left(g_2^2 W_{\mu\nu}^a \widetilde{W}^{a\mu\nu} - g_1^2 B_{\mu\nu} \widetilde{B}^{\mu\nu} \right) - V(\phi, \Phi_H^\dagger \Phi_H) \end{aligned} \quad (3.8)$$

where g_1 and g_2 are the U(1) and SU(2) coupling constants, respectively, and \mathcal{D}_μ is the usual covariant derivative. The coupling to gauge bosons above prevents the relaxion to couple to the $\gamma\tilde{\gamma}$ and has to be protected by a symmetry in a UV model containing the SM group. An example of such a UV completion is discussed in [10], where the coupling structure $\phi(\theta_W W\widetilde{W} + \theta_B B\widetilde{B})$ with $\theta_W = -\theta_B$ is fixed if the SM is embedded in a left-right symmetric model $SU(2)_L \times SU(2)_R \times U(1)_{B-L}$ (see e.g [48–51]). In this case, a global PQ symmetry forces the coupling structure as in Eq. (3.8) and then forbids the relaxion coupling to $\gamma\tilde{\gamma}$. The coupling structure which prevents a coupling of the relaxion to the photon also appears in non-minimal composite Higgs models with coset $SO(6)/SO(5)$ where the interaction of the additional singlet PNGB arising via anomalies is of the form (3.8) with no coupling to the photon [52–55].

On the other hand, shift symmetry breaking terms like $\sim g'\Lambda\phi h^2$ in Eq. (2.1) do not respect this global PQ symmetry, so an anomalous interaction with photons can be generated through the small mixing with the Higgs. One should then guarantee that the mixing is sufficiently suppressed so that the coupling $\propto (\phi/f_\gamma)\tilde{\gamma}\gamma$ is harmless to the mechanism. Note that such an effective anomalous coupling to photons is also present in other relaxion models, implying that an exponential particle production can also be present in other constructions. There are two reasons why this coupling can be dangerous. First, if photon production is efficient, the corresponding friction term which is always active should be included in the relaxion evolution. Second, these photons may generate a temperature that is large enough to deconfine the strong sector which is supposed to stop the relaxion field evolution through the generation of the potential barriers. Finally, if such temperature is large ($T_\gamma \gtrsim \Lambda$), we may end up scanning the Higgs thermal mass instead of the vacuum mass parameter μ_h^2 .

The coupling $(\phi/f_\gamma)\tilde{\gamma}\gamma$ is generated through the mixing with the Higgs (see Sec. 5.1), which decays into two photons with a CP-violating coupling that is generated at three loops. It is suppressed by one power of the SM Jarlskog invariant $J = \text{Im}[V_{ij}V_{kl}V_{il}^*V_{kj}^*] \sim 10^{-5}$ [56]. Its size can be estimated as

$$\frac{1}{f_\gamma} \sim \frac{g' J}{h} \frac{\alpha_W^2 \alpha_{\text{em}}}{(4\pi)^6} \quad (3.9)$$

where $h \sim \Lambda$ is the Higgs VEV during the relaxation process, α_{em} is the fine-structure constant and $\alpha_W = \alpha_{\text{em}}/\sin^2 \theta_W$ with θ_W being the SM weak angle. The particle production rate $\dot{\phi}/f_\gamma \sim \Lambda^2/f_\gamma$ (see below) should be smaller than the Hubble rate $H \sim \Lambda^2/M_{\text{Pl}}$ that gives the dilution rate of these photons due to cosmic expansion. Given the smallness of the prefactor in Eq. (3.9), this bound is trivially satisfied.⁶

After EW symmetry breaking, we can rewrite the relevant part of Eq. (3.8) in terms of the mass eigenstates A_μ, Z_μ, W_μ^\pm

$$\mathcal{L} \supset m_W^2(h) W_\mu^- W^{+\mu} + \frac{1}{2} m_Z(h)^2 Z_\mu Z^\mu$$

⁶In addition, as the relaxion mixes with the Higgs, one can generate the term $\sim \alpha_V/(4\pi)g'(\Lambda/v_{\text{EW}})\phi/f F_{\mu\nu}F^{\mu\nu}$ using a fermion loop, which contributes to the vectors' kinetic term. Using $\phi \sim \Lambda/g'$ and $f \sim \Lambda^2/(2m_Z)$ (see Eq. (4.3)), one can see that such contribution is sub-dominant compared to the canonical kinetic term.

$$-\frac{\phi}{f}\epsilon^{\mu\nu\rho\sigma}(2g_2^2\partial_\mu W_\nu^- \partial_\rho W_\sigma^+ + (g_2^2 - g_1^2)\partial_\mu Z_\nu \partial_\rho Z_\sigma - 2g_1g_2\partial_\mu Z_\nu \partial_\rho A_\sigma) , \quad (3.10)$$

where the masses of the gauge bosons are $m_W(h) = g_2 h/2$ and $m_Z(h) = \sqrt{g_2^2 + g_1^2}h/2$. The contribution of the WW and of the ZA terms can be safely neglected when discussing the evolution of the relaxion and the particle production phase. Indeed, we expect the WW contribution to be suppressed by thermal effects, due to its non-abelian nature [57–59]. The photon, instead, does not present a tachyonic instability in its equation of motion, and we expect its behaviour to be oscillatory up to the critical point when the Z field starts growing. After this point, one of the two components of the field will grow following the evolution of the Z , while the other will decrease. Since this behaviour will only start after the critical point, we expect the photon to contribute at most with a $\mathcal{O}(1)$ factor to our results.

A massive vector field V_μ can be decomposed in three independent parts: two transverse components and one longitudinal component. The term $F_{\mu\nu}\tilde{F}^{\mu\nu}$ does not contain the longitudinal one, whose equation of motion is therefore the usual Klein-Gordon equation with a positive mass term, plus an additional term that encodes the variation of the mass. Because this equation does not predict a tachyonic growth, we can neglect the longitudinal mode in our description. As shown in App. A.2, absorbing the gauge couplings in the definition of f , the equations of motion for the relaxion, the Higgs, and the transverse modes of the vector fields are:

$$\ddot{\phi} - g\Lambda^3 + g'\Lambda h^2 + \frac{\Lambda_b^4}{f'} \sin \frac{\phi}{f'} + \frac{1}{4f} \langle F\tilde{F} \rangle = 0 \quad (3.11)$$

$$\ddot{h} + (g'\Lambda\phi - \Lambda^2)h + \lambda h^3 - \frac{1}{2}g_V^2 \langle V_\mu V^\mu \rangle h = 0 \quad (3.12)$$

$$\ddot{V}_\pm + (k^2 + m_V^2 \mp k \frac{\dot{\phi}}{f}) V_\pm = 0 \quad (3.13)$$

where

$$m_V^2 = g_V^2 h^2, \quad (3.14)$$

and we have neglected the spatial fluctuations of h and ϕ . We also define

$$\omega_{k\pm}^2 = k^2 + m_V^2 \mp k \frac{\dot{\phi}}{f}. \quad (3.15)$$

Notice that, for simplicity, we are working in Minkowski space. This simplification is well justified, since the particle production process is very fast, as we will see shortly, and cosmic expansion can be neglected. The quantities in brackets should be interpreted as the expectation values of the corresponding quantum operators (see the derivation in App. A.2):

$$\langle F\tilde{F} \rangle = \frac{1}{4\pi^2} \int dk k^3 \frac{\partial}{\partial t} (|V_+|^2 - |V_-|^2). \quad (3.16)$$

When the Higgs VEV (and consequently the mass of the gauge bosons) decreases, Eq. (3.13) exhibits a tachyonic instability for the V_+ polarization, in some range of k . The first mode k_* that becomes tachyonic is the one for which $\omega_{k\pm}^2$ is minimum, *i.e.*

$$0 = \frac{d}{dk} (k^2 + m_V^2 - k \frac{\dot{\phi}}{f}) \Big|_{k=k_*} = 2k_* - \frac{\dot{\phi}}{f} \implies k_* = \frac{\dot{\phi}}{2f} \quad (3.17)$$

Plugging this into the equation of motion we get

$$\ddot{V}_+ + (m_V^2 - \frac{\dot{\phi}^2}{4f^2}) V_+ = 0 \quad (3.18)$$

that becomes tachyonic for⁷

$$\dot{\phi} \gtrsim \dot{\phi}_c = 2f m_V . \quad (3.19)$$

We call t_c the time when this condition turns true. Initially, the velocity is large enough that the field jumps over the barriers. At the time $t = t_c$, the terms $\langle F\tilde{F} \rangle$ and $\langle VV \rangle$ in the equations of motion grow exponentially. Particle production starts. The term $\langle F\tilde{F} \rangle/4f$ comes to dominate the equation of motion of ϕ , which slows down and is captured in the potential wells.⁸ The parameters of the model must be chosen in such a way that, at t_c , the relaxion field is as close as possible to the critical value Λ/g' , thus generating the hierarchy between the cutoff Λ and the electroweak scale. Numerical solutions to the system of equations (3.11, 3.12, 3.13) are shown for illustration in Fig. 15 in App. A. The plotted time evolution is limited to a range where numerics is under control (shortly after t_c , fields are subject to a large oscillatory behaviour). This is enough to see that the relaxion slows down and ϕ stops growing, as soon as

$$h(t) < \dot{\phi}/(2g_V f) , \quad (3.20)$$

which is when some k modes becomes tachyonic ($\omega_{k+}^2 < 0$), stabilising the Higgs mass parameter, while the temporary additional contribution to the Higgs mass parameter from the gauge field production grows.

A crucial role is played by the evolution of the Higgs field right after particle production starts. Two main effects should be considered here. First, as the V_+ field grows, the $\langle VV \rangle$ term in Eq. (3.12) induces a positive mass term for the Higgs field, temporarily restoring the electroweak symmetry. The field h rapidly rolls to zero, and so does the mass of the vector boson, making the tachyonic growth even faster. Another effect, which on the other hand is not included in the system (3.11, 3.12, 3.13), is due to the temperature. The produced particles are expected to thermalise, generating an additional thermal mass term for the Higgs, which adds to the one

⁷Note that the tachyonic instability should turn on before the relaxion reaches the critical value Λ/g' which is when the EW symmetry is recovered. To simplify the notation, we do not make a distinction between Λ/g' and the point where the first mode becomes tachyonic (given in (3.18)) as these points are very close to each other compared to the evolution range.

⁸Notice that the intuition of $\langle F\tilde{F} \rangle$ acting as a friction term which is valid in inflationary models as in [47] does not apply here, since it is derived from the assumption of a constant slow-roll velocity.

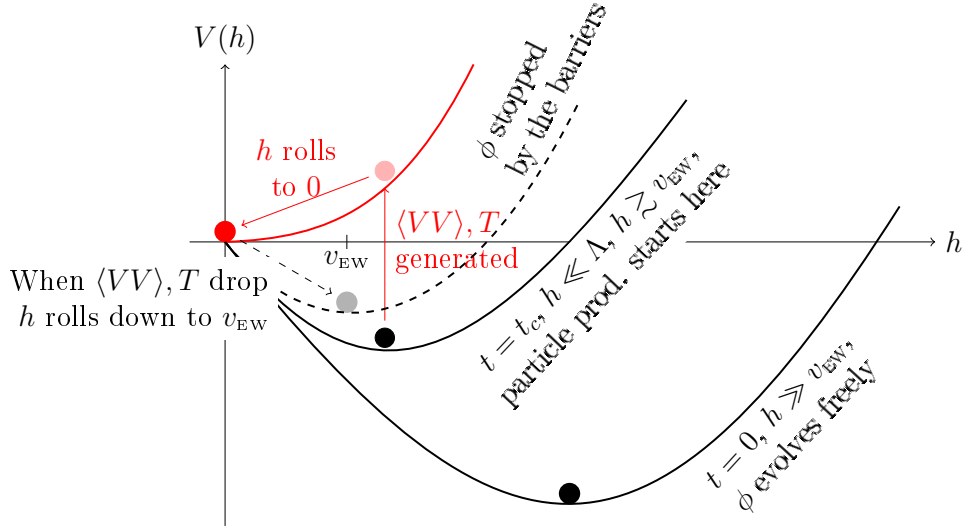


Figure 6. Evolution of the Higgs field during cosmological relaxation intertwined with gauge boson production.

mentioned above. After temperature has dropped, the Higgs relaxes to the minimum of the $T = 0$ potential, which is now given by v_{EW} . Such evolution of the Higgs field is summarised in Fig. 6.

The thermalisation process and the computation of the reheating temperature are a topic of study in their own that goes beyond the scope of this paper. On the other hand, the time scale for particle production in the presence of a thermal bath can be estimated as follows [10]. The generation of a thermal mass for the Higgs is not the only effect of thermalisation. The production of gauge bosons will be affected by the presence of the thermal plasma, and the dispersion relation for the tachyonic mode (V_+) is modified into

$$\omega^2 = k^2 + m_V^2 - k \frac{\dot{\phi}}{f} + \Pi[\omega, k] \quad (3.21)$$

where, in a hard thermal loop (*i.e.* high temperature) limit [60],

$$\Pi[\omega, k] = m_D^2 \frac{\omega}{k} \left(\frac{\omega}{k} + \frac{1}{2} \left(1 - \frac{\omega^2}{k^2} \right) \log \frac{\omega + k}{\omega - k} \right). \quad (3.22)$$

Here $m_D^2 = g_{\text{EW}}^2 T^2 / 6$ is the Debye mass of the plasma. In pure QED, it comes from evaluating an electron loop and it is proportional to the coupling e^2 . Doing the same calculation but including all SM fermions (all assumed to be light in this phase), one gets a factor $g_1^2 \times ((-1)^2 \times 3 + (2/3)^2 \times 3 \times 3 + (-1/3)^2 \times 3 \times 3) = (32/9)g_1^2$, where g_1 is the SM hypercharge coupling. This result should be multiplied by $\sin^2 \theta_W \approx 0.23$ to project the Z onto its abelian component. Taking the value of the SM coupling $g_1 \approx 0.5$ we get $g_{\text{EW}}^2 \approx 0.2$.

For imaginary frequency $\omega = i\Omega$ the function $\Pi[\omega, k]$ is positive, which already shows that the tachyonic instability is damped by the thermal bath. As we discussed above, the instability first develops for $k \sim \dot{\phi}/(2f)$, and its timescale Ω is initially small. For $\Omega/k \rightarrow 0$ we can expand Eq. (3.22) obtaining

$$\Pi[\Omega, k] \approx \frac{\pi}{2} \frac{|\Omega|}{k} m_D^2. \quad (3.23)$$

Plugging this back in Eq. (3.21) and neglecting the bare mass m_V and $\mathcal{O}(\Omega^2)$ terms we obtain that Ω is maximized for $k = 2\dot{\phi}/(3f)$,

$$\Omega_{\max} \approx \frac{8}{27\pi} \frac{\dot{\phi}^3}{f^3 m_D^2} = \frac{16}{9\pi g_{\text{EW}}^2} \frac{\dot{\phi}^3}{T^2 f^3}. \quad (3.24)$$

Equation (3.24) gives an estimate of the typical timescale for the exponential growth of the Fourier modes of the vector field V_+ in the presence of a thermal bath,

$$\Delta t_{\text{pp}} \sim \frac{9\pi g_{\text{EW}}^2}{16} \frac{T^2 f^3}{\dot{\phi}^3}, \quad (3.25)$$

which we are going to use in the following sections in quantifying the efficiency of the mechanism.

4 Parameter space for successful relaxation of the EW scale through gauge bosons production

In the following we list all the constraints imposed to realize the relaxion idea using gauge bosons production as a stopping mechanism.

1. **Higgs field tracking the minimum of its potential:** According to the discussion in Sec. 2.3, the Higgs stops tracking its minimum when $h \sim (g'\Lambda\dot{\phi})^{1/3}/\sqrt{\lambda}$ as in Eq. (2.19). We need to guarantee that this condition only breaks down when the Higgs field value is already below the electroweak scale, i.e. $h \lesssim v_{\text{EW}}$. This translates into

$$g' \lesssim \left(\frac{v_{\text{EW}} \sqrt{\lambda}}{\Lambda} \right)^3, \quad (4.1)$$

where we neglect particle production and assume $\dot{\phi} \sim \Lambda^2$.

2. **Prediction for the electroweak scale:** To obtain the correct electroweak scale, the dissipation should be important when the mass of the gauge boson is close to m_Z

$$\dot{\phi}_c \sim 2m_Z f, \quad (4.2)$$

where $\dot{\phi}_c$ is the velocity when particle production becomes efficient (see the discussion in Sec. 3.2). For the consistency of the effective theory we expect that $\dot{\phi}$

does not exceed Λ^2 . Assuming a non-vanishing initial velocity, after traveling an entire field range Λ/g' , the velocity would be $\dot{\phi} \sim \Lambda^2$. Therefore, we can expect the final mass of the gauge bosons to be

$$m_Z \sim \frac{\Lambda^2}{2f}. \quad (4.3)$$

On the other hand, during its rolling phase the field must be able to jump over the barriers, and therefore $\dot{\phi} \gtrsim \Lambda_b^2$. For this reason we assume

$$\Lambda_b \lesssim \Lambda. \quad (4.4)$$

3. **Stopping condition:** Once particle creation slows down the relaxion, the constant barrier of the cosine potential ($\sim \Lambda_b^4 \cos(\phi/f')$) should be able to stop the field by cancelling the slope:

$$\Lambda_b^4 \gtrsim g \Lambda^3 f'. \quad (4.5)$$

4. **Scanning precision:** the scanning of the Higgs mass should have enough precision so that we do not overshoot the electroweak scale,

$$g' \Lambda \delta\phi = g' \Lambda (2\pi f') \lesssim m_h^2. \quad (4.6)$$

5. **Efficient energy dissipation:** We need to impose that the kinetic energy that the relaxion loses due to particle production is larger than the one it gains by rolling down the potential slope,

$$\Delta K_{\text{rolling}} \lesssim \Delta K_{\text{pp}}. \quad (4.7)$$

We assume that a $\mathcal{O}(1)$ fraction of the kinetic energy is dissipated away by particle creation, meaning that $\Delta K_{\text{pp}} \sim \dot{\phi}^2/2$. The energy gained by rolling can be estimated as $\Delta K_{\text{rolling}} \sim \frac{dK}{dt} \Delta t_{\text{pp}}$, where $dK/dt = -dV/dt \sim g\Lambda^3 \dot{\phi}$. To consider the most stringent bound, we evaluate this condition for $\dot{\phi}^2/2 = \dot{\phi}_{\text{stop}}^2/2 \sim \Lambda_b^4$, the maximum velocity the relaxion can have after it has been trapped. We get

$$\frac{9\pi g_{\text{EW}}^2}{16} T^2 f^3 \lesssim \frac{2\Lambda_b^8}{g\Lambda^3}. \quad (4.8)$$

Evaluating the condition at $\dot{\phi}_c$ would lead to a similar bound on Λ , but would fail at constraining the scenario with $\Lambda_b \ll \Lambda$, which, as we will see, is excluded through Eq. 4.8.

6. **Small variation of the Higgs mass:** When ϕ is loosing its kinetic energy, the Higgs mass parameter should not vary more than a fraction of the electroweak scale during the time it takes for the relaxion velocity to become smaller than the barrier. This can be satisfied if we impose

$$\Delta m_h \sim \frac{\Delta m_h^2}{m_h} \sim \frac{1}{m_h} g' \Lambda \dot{\phi} \Delta t_{\text{pp}} \lesssim m_h, \quad (4.9)$$

which, again, we evaluate at $\dot{\phi} = \dot{\phi}_{\text{stop}} \sim \Lambda_b^2$ to derive the most stringent bound.

7. **Shift symmetry not restored:** After the relaxion has been trapped, the temperature may be larger than the condensation scale of the cosine potential. In this case, the potential barriers would disappear, and the relaxion would start rolling again until the temperature is redshifted enough for the barriers to be generated again. To avoid this scenario, we impose that

$$T < \Lambda_b. \quad (4.10)$$

This condition only applies when the sector which generates the barriers is in thermal equilibrium with the SM. Assuming that the barriers are generated by some QCD-like gauge group coupled to the relaxion as $\phi G\tilde{G}/f'$, we naively estimate the rate for $gg \leftrightarrow ZZ$ interactions mediated by the relaxion as $\Gamma \sim T^5/(f^2 f'^2)$, which must be larger than the Hubble rate $H \sim \Lambda^2/M_{\text{Pl}}$.

We now want to combine all the above constraints. To display the allowed region of parameter space, we make a few simplifying assumptions. First, we assume $g = g'$, keeping in mind that from the perspective of a UV completion the terms proportional to g' and g in Eq. (2.1) should be generated in a similar way. Secondly, we assume that a $\mathcal{O}(1)$ fraction of the relaxion kinetic energy is converted into radiation with temperature given by

$$\frac{\dot{\phi}_c^2}{2} \sim \frac{\pi^2}{30} g_* T_{\text{pp}}^4, \quad (4.11)$$

where g_* is the number of relativistic degrees of freedom in the SM at high temperature, and $\dot{\phi}_c \sim \Lambda^2$. Finally, from Eq. (4.3) we assume

$$f = \Lambda^2/(2m_Z). \quad (4.12)$$

Under these assumptions, the relations 1 to 7 together with the condition that the relaxion does not drive another period of inflation (see Eq. (2.9) in Sec. 2.1) can be conveniently written as:

$$g' \gtrsim 0.2 \frac{\Lambda}{M_{\text{Pl}}} \quad \text{Avoid slow-roll} \quad (4.13)$$

$$g' \lesssim \left(\frac{v_{\text{EW}} \sqrt{\lambda}}{\Lambda} \right)^3 \quad \text{Higgs tracking the minimum} \quad (4.14)$$

$$\Lambda_b \lesssim \Lambda \quad \phi \text{ initially rolls above the barriers} \quad (4.15)$$

$$g' \lesssim \frac{\Lambda_b^4}{\Lambda^3 f'} \quad \text{The barriers are high enough to stop } \phi \quad (4.16)$$

$$g' \lesssim \frac{m_h^2}{2\pi f' \Lambda} \quad \text{Precision of the mass scanning} \quad (4.17)$$

$$\Lambda_b^8 \gtrsim 0.1 \frac{g_{\text{EW}}^2}{g_*^{1/2}} \frac{g' \Lambda^{11}}{m_Z^3} \quad \text{Efficient dissipation} \quad (4.18)$$

$$\Lambda_b^4 \gtrsim 0.1 \frac{g_{\text{EW}}^2}{g_*^{1/2}} \frac{g' \Lambda^9}{m_h^2 m_Z^3} \quad \text{Small Higgs mass variation} \quad (4.19)$$

$$\Lambda_b \lesssim f' \quad \text{Consistency of symmetry breaking pattern} \quad (4.20)$$

$$\Lambda \lesssim f' \quad \text{EFT validity} \quad (4.21)$$

$$g' \lesssim 7 \frac{g_*^{1/2}}{g_{\text{EW}}^2} \frac{m_Z^3}{\Lambda^3} \quad \text{Combining (4.15) and (4.18)} \quad (4.22)$$

$$g' \lesssim 7 \frac{g_*^{1/2}}{g_{\text{EW}}^2} \frac{m_h^2 m_Z^3}{\Lambda^5} \quad \text{Combining (4.15) and (4.19)} \quad (4.23)$$

$$f'^2 \gtrsim 12 \frac{M_{\text{Pl}} m_Z^2}{g_*^{5/4} \Lambda} \text{ or } \Lambda_b \gtrsim \frac{\Lambda}{g_*^{1/4}} \quad \text{No symmetry restoration} \quad (4.24)$$

We used Eqs. (4.13), (4.14), (4.22) and (4.23) to constrain the parameters Λ and g' . Note that, while Eqs. (4.13) and (4.14) are generic, Eqs. (4.22) and (4.23) depend on our assumptions on the behaviour of the gauge bosons after thermalisation, which is a difficult subject that would require a careful treatment beyond our simple description. Our choice was to maximize the strength of these constraints, therefore the reader should remember that they could in principle be relaxed. Despite all these constraints, interestingly, there is a sizeable region of parameter space that remains open. In Fig. 7 we show the bounds on Λ and g' that are drawn from the above inequalities. The maximum cutoff that we can obtain in our model is

$$\Lambda \sim 3 \times 10^5 \text{ GeV} , \quad (4.25)$$

that can be extended up to $\Lambda \sim 10^6 \text{ GeV}$ in the case reheating is very inefficient. In the right plot, we compare this open region with the parameter regions associated with the original relaxion models implemented during a long inflation era. The relaxion mechanism relying on gauge boson production as a source of friction is associated with much larger values of the coupling g' .

We also chose five benchmark points within the allowed region, and used Eqs. (4.15)–(4.21) and (4.24) to constrain the remaining free parameters Λ_b and f' in each of these cases:

$$\begin{aligned} \text{scenario A:} \quad & \Lambda = 10^4 \text{ GeV}, \quad g' = 3 \times 10^{-15} \\ \text{scenario B:} \quad & \Lambda = 10^4 \text{ GeV}, \quad g' = 3 \times 10^{-9} \\ \text{scenario C:} \quad & \Lambda = 4 \times 10^4 \text{ GeV}, \quad g' = 10^{-13} \\ \text{scenario D:} \quad & \Lambda = 10^5 \text{ GeV}, \quad g' = 3 \times 10^{-14} \\ \text{scenario E:} \quad & \Lambda = 7 \times 10^5 \text{ GeV}, \quad g' = 2 \times 10^{-13}. \end{aligned} \quad (4.26)$$

Figure 8 shows the constraints on the $f' - \Lambda_b$ plane for the benchmark cases listed above. Notice that benchmark E is excluded if we assume that the vector bosons efficiently thermalise. Again, conditions (4.18), (4.19), and (4.24) depend on the details of the thermalisation process and should be considered as a pessimistic bound. The results in Fig. 8 indicate that, in order for the mechanism to work, we need to require a coincidence of scales $\Lambda \sim \Lambda_b$, which may be reasonable if those two scales are generated by a common dynamics.

On top of these constraints, one should also check that particle production happens on a timescale shorter than a Hubble time, in order to justify our assumption of

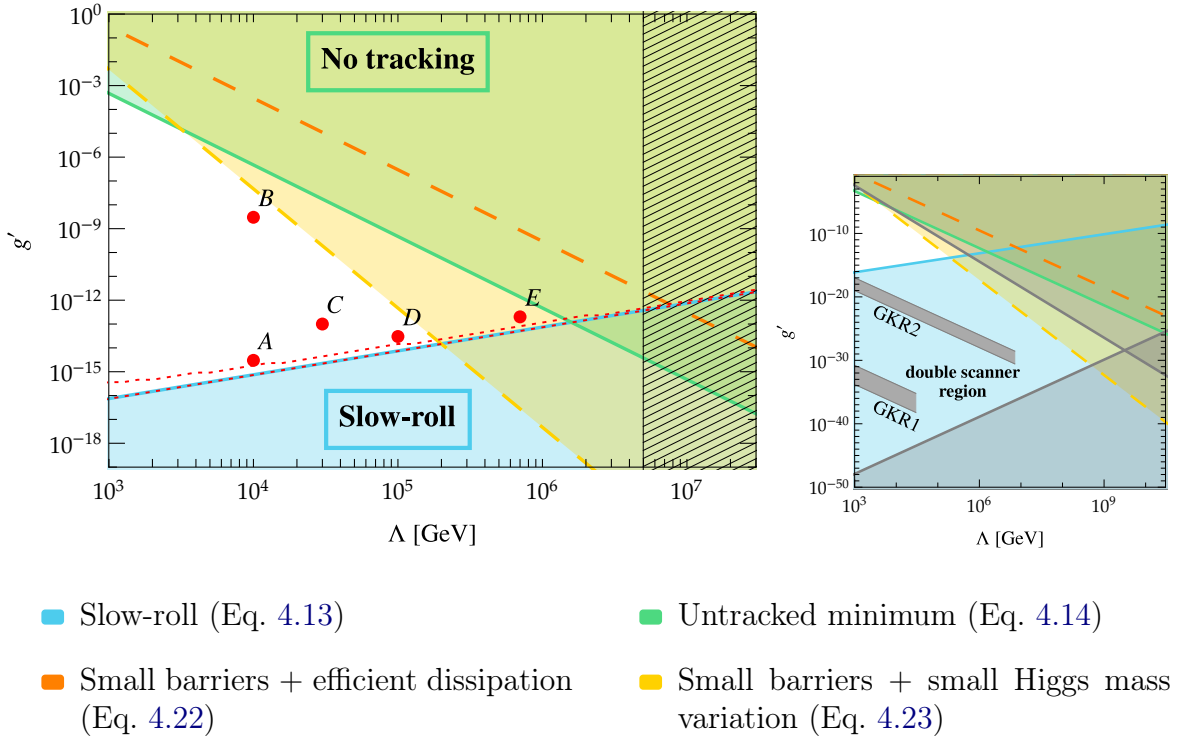


Figure 7. Summary of the available region of parameter space in the $g' - \Lambda$ plane consistent with the relaxion mechanism exploiting particle production instead of inflation. Constraints come from Eqs. (4.13), (4.14), (4.22) and (4.23). The red dots correspond to the five benchmark cases of Fig. 8. The dashed lines correspond to the bounds which rely on conservative assumptions about the thermalisation process. The region between the red dotted lines corresponds to the one in which the inflaton is allowed to reheat the SM before relaxation takes place (see Fig. 3). The rectangular hashed region at large Λ is the one in which the approximation of instantaneous particle production fails. Right plot: This smaller plot indicates in comparison the parameter space relevant for the two original relaxion models (GKR1 for the relaxion being the QCD axion and GKR2 for the model with strong dynamics at the weak scale) proposed in [1]) as well as for the double-scanner mechanism of Ref. [2], which all use inflation as a source of friction.

a Minkowski metric. During the whole relaxation process the relaxion dominates the energy density of the universe, with $H \sim \Lambda^2/M_{\text{Pl}}$. Therefore we get the relation

$$\Delta t_{\text{pp}} \sim \frac{9\pi g_{\text{EW}}^2}{16} \frac{T^2 f^3}{\dot{\phi}^3} \lesssim \frac{M_{\text{Pl}}}{\Lambda^2} \quad (4.27)$$

which, for $\dot{\phi} \sim \Lambda^2$, is satisfied for $\Lambda \lesssim 7 \times 10^6 \text{ GeV}$. The region where the Minkowski approximation breaks down is shown in Fig. 7 with a hashed area.

In our setup, the total field excursion over the decay constant $\Delta\phi/f' \sim \Lambda/(g'f')$ remains typically large, as shown in Fig. 9, making a possible embedding of this model in string theory problematic, as discussed in [8].

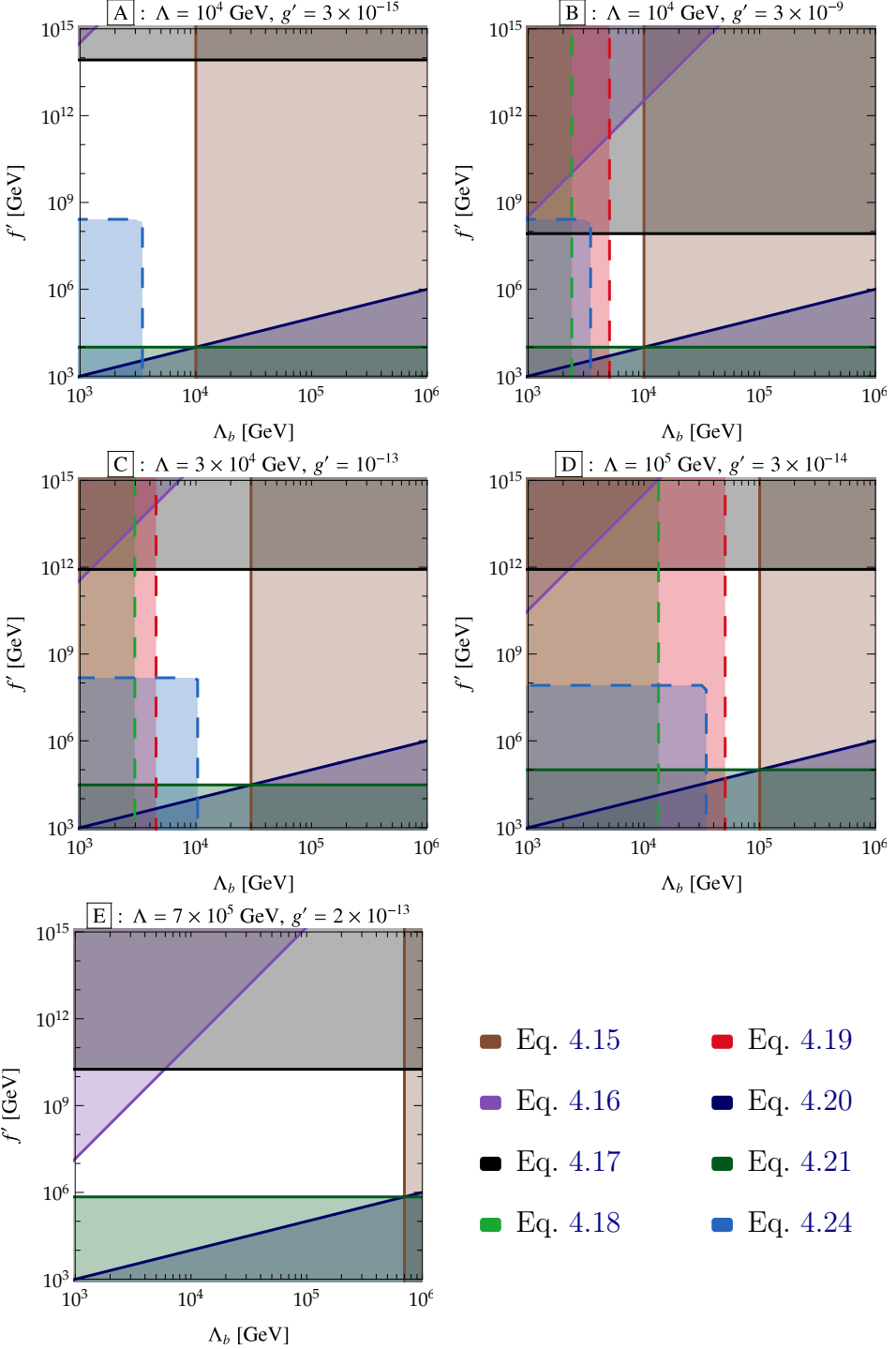


Figure 8. Constraints on the f' - Λ_b plane from Eqs. (4.15)–(4.20), (4.24) for the five benchmark cases listed in Eq. (4.26). The dashed lines correspond to the bounds which rely on conservative assumptions about the thermalisation process.

At this stage, we now need to consider phenomenological constraints and see whether they limit further the parameter space. For this, we determine the relaxion

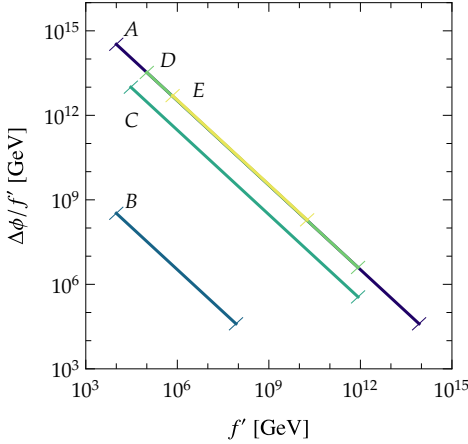


Figure 9. Ratio of the total field excursion $\Delta\phi \sim \Lambda/g'$ over the decay constant f' , for the five benchmarks defined in Eq. 4.26. The lines are cut at the allowed values of f' .

mass and lifetime in the next section.

5 Relaxion properties

5.1 Relaxion mass and mixing with the Higgs

After the field ϕ has relaxed at one of the potential's minima, its mixing angle with the Higgs is obtained by expanding around the minimum of the potential ϕ_0

$$V(\phi, h) \supset -g\Lambda^3\phi + \frac{1}{2}[-\Lambda^2 + g'\Lambda(\phi_0 + \phi)]h^2 + \frac{\lambda}{4}h^4 + \frac{1}{2}m_\phi^2\phi^2, \quad (5.1)$$

where we now call ϕ the field displacement which is smaller than f' . The mass of the relaxion is

$$m_\phi \sim \Lambda_b^2/f' \quad (5.2)$$

and is obtained by expanding the cosine potential. A contour plot of m_ϕ is shown in Fig. 10. The allowed mass range depends, given the values of Λ and g' , on the intersection of the conditions displayed above. In particular, the maximal m_ϕ is obtained from Eqs. (4.15), (4.20) and (4.21), which imply $m_\phi \lesssim \Lambda$, consistently with the fact that Λ represents the cutoff of the theory. The allowed mass ranges for the five benchmark points of Eq. (4.26) are approximately given by

$$\begin{aligned} \text{scenario A: } & m_\phi \in [10 \text{ eV}, 10 \text{ TeV}] \\ \text{scenario B: } & m_\phi \in [300 \text{ MeV}, 10 \text{ TeV}] \\ \text{scenario C: } & m_\phi \in [20 \text{ keV}, 30 \text{ TeV}] \\ \text{scenario D: } & m_\phi \in [3 \text{ MeV}, 100 \text{ TeV}] \\ \text{scenario E: } & m_\phi \in [2 \text{ MeV}, 700 \text{ TeV}] \end{aligned} \quad (5.3)$$

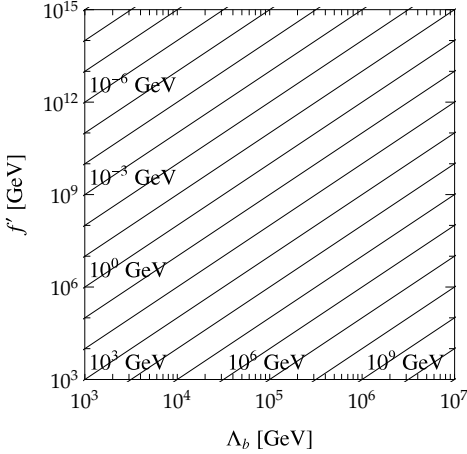


Figure 10. Contours of m_ϕ in the f' – Λ_b plane. The thick lines correspond to the indicated labels.

In our scenario, the barriers do not depend on the Higgs VEV and the scale where this potential is generated can be as high as the cutoff ($\Lambda_b \lesssim \Lambda$). This implies that the upper bounds for the mass ranges in (5.3) can be much higher than the ones obtained in the relaxion models with a Higgs-dependent barrier (see e.g. [2, 33–35]). Additionally, as we shall see in Sec. 6, most of the lower bounds above are going to be shifted to higher masses after we consider the cosmological constraints.

Given the potential in Eq. (5.1), one can compute the mixing angle of the relaxion with the Higgs as

$$\sin 2\theta = \frac{2g'\Lambda v_{\text{EW}}}{\sqrt{4g'^2\Lambda^2 v_{\text{EW}}^2 + (m_h^2 - m_\phi^2)^2}}. \quad (5.4)$$

The mixing angle θ has a maximum of $\pi/4$ for $m_\phi = m_h$, which is a condition that can be realized in our model. Apart from a very narrow region (typically fractions of MeV) around this point, the mixing angle is $\theta \ll 1$, and we can safely approximate $\sin 2\theta$ with 2θ . Let us briefly notice here that the VEV of the relaxion field is automatically smaller than f' once condition (4.5) is taken into account. Figure 12 shows a plot of the angle $\sin 2\theta$.

Additional contribution to the Higgs-relaxion mixing can be obtained by considering a diagram in which the bosonic lines of the $\phi F\tilde{F}$ and $hZ_\mu Z^\mu$ vertices are connected via a fermion box. The corresponding mixing term can be estimated as $Jv_{\text{EW}}^4 f^{-2} (4\pi)^{-6}$, with $J = \text{Im}[V_{ij}V_{kl}V_{il}^*V_{kj}^*] \sim 10^{-5}$ being the Jarlskog invariant [56], which is suppressed compared to the above contribution in all the relevant parameter space.

The smallness of the mixing angle makes collider searches essentially harmless in our model. As an example, we considered the production of ϕ particles at the LHC through its mixing with the Higgs, and its subsequent decay in the $Z\gamma$ channel. The predicted cross section turns out to be roughly $10 - 15$ orders of magnitude smaller than the limit from [61]. Furthermore, as the relaxion mixes with the Higgs, it can be

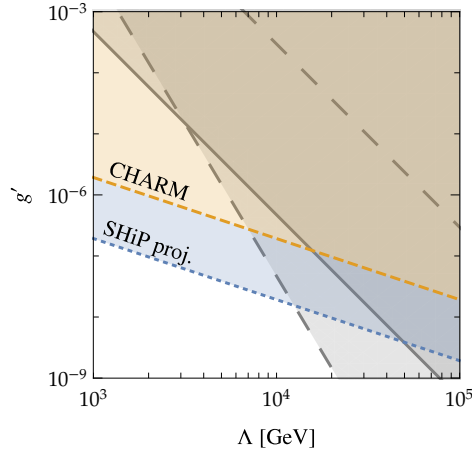


Figure 11. Region where CHARM ($m_\phi \in [0.20 \text{ GeV}, 0.35 \text{ GeV}]$) and SHiP ($m_\phi \in [0.20 \text{ GeV}, 4 \text{ GeV}]$) can probe part of the $f' - \Lambda_b$ parameter space.

produced in rare decays of kaons and B -mesons, which are constrained by flavor and beam dump experiments. We consider bounds on the relaxion-Higgs mixing from the CHARM experiment given in [62] which can probe relaxion masses in the range $m_\phi \in [0.20 \text{ GeV}, 0.35 \text{ GeV}]$. Similarly, the future SHiP experiment can probe the relaxion in the range $m_\phi \in [0.20 \text{ GeV}, 4 \text{ GeV}]$, as shown in Fig. 11. In addition, we checked that flavor constraints for the mixing for relaxion masses from MeV to 5 GeV cannot constrain our parameter space as our mixing angle is below the current bounds [34].

Interestingly, the same anomalous structure in Eq. (3.8) appears in composite Higgs models based on the coset $SO(6)/SO(5)$ [52–55]. In addition to the Higgs doublet, this theory contains another PNGB state, which, at leading order, has an interaction with the SM gauge bosons of the form of the $\phi F\tilde{F}$ coupling in Eq. (3.8).⁹ The production mechanism of this PNGB via the topological interactions was studied in Ref. [54]. We consider the reach at 100 TeV FCC-pp with a luminosity of 3 ab^{-1} given in [54], which can exclude with 95% C.L. cutoff scales below $\Lambda \lesssim 5 \times 10^3 \text{ GeV}$ for fixed mass $m_\phi = 1 \text{ TeV}$. This is below the minimal cutoff scale we consider in our benchmark scenarios which is $\Lambda = 10^4 \text{ GeV}$ (scenarios A and B) so that given the study in [54] our relevant parameter space appears to be beyond the reach of the 100 TeV FCC-pp.

5.2 Relaxion lifetime

Bounds on the properties of the relaxion field can come from its decay to SM particles after the relaxation mechanism took place. The decay can proceed both through the mixing of ϕ with the Higgs boson or through its coupling to $F\tilde{F}$, where the second channel is forbidden when $m_\phi < m_Z$. Below m_Z , the perturbative decay width is given

⁹This motivates the investigation of UV completions for the relaxation mechanism with particle production in the context of composite Higgs models [63].

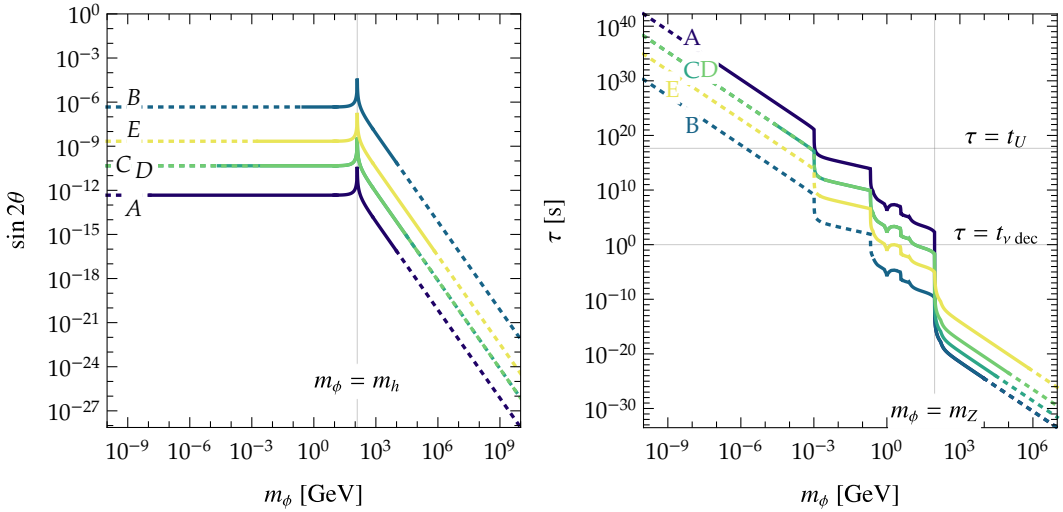


Figure 12. Relaxion–Higgs mixing angle and relaxion lifetime, for scenarios A–E defined in Eq. (4.26). The solid lines correspond to the mass range allowed in our model once the constraints discussed previously are applied, see Eq. (5.3). *Left:* Mixing angle. *Right:* Lifetime. For reference we indicate the vertical line $m_\phi = m_Z$ where the $\phi \rightarrow Z\gamma$ opens up, and the two horizontal lines correspond to the age of the universe t_U and the time of neutrino decoupling $t_{\nu \text{dec}}$, respectively.

by

$$\Gamma_\phi = \theta^2 \Gamma_h(m_\phi), \quad (5.5)$$

where $\Gamma_h(m_\phi)$ is the decay width of a Higgs boson with mass m_ϕ . For this width we took the results of [64]. Above m_Z , the $Z\gamma$ channel opens, followed by the WW and ZZ ones. These decays proceed mostly through the $F\tilde{F}$ coupling, while the mixing angle suppresses the decay through the Higgs couplings. The relaxion lifetime is shown in Fig. 12, for the five benchmark scenarios.

Note that for the relaxion not to couple to photons, the corresponding UV completions should not generate couplings to light fermions of the type $\partial_\mu \phi (\bar{\psi} \gamma^\mu \gamma_5 \psi) / f$ either. Only a very specific combination like $\partial_\mu \phi (J_{e^c}^\mu - J_{\tau^c}^\mu) / f$ would not reintroduce the anomalous coupling to the photon [10]. It would however shorten the lifetime of the relaxion at small masses and therefore weaken the cosmological bounds discussed in the next section. We do not consider this possibility further.

6 Cosmological constraints

After the relaxation process has ended, a population of ϕ particles is left in the universe that may lead to important cosmological observations. Depending on the lifetime of the relaxion, it may either lead to overabundance of dark matter in the universe or ruin the predictions of Big Bang nucleosynthesis. In this section, we derive the corresponding bounds on the relaxion parameter space.

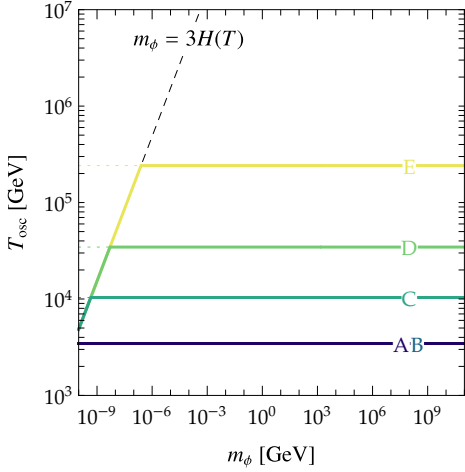


Figure 13. Temperature at the onset of oscillations for the different scenarios. The black line shows the condition $m_\phi = 3H(T)$, that determines the initial temperature only at very low masses.

6.1 Relaxion abundance in the early universe

The population of ϕ particles is generated through two main mechanisms: vacuum misalignment and thermal production via the Primakoff process.

6.1.1 Vacuum misalignment

After the relaxion has been trapped in one of the minima of the potential, it will start oscillating with an amplitude that decreases with time due to the cosmological expansion and to the further production of gauge bosons, at least as far as its velocity is large enough. When the amplitude falls below a value that we are going to estimate in the following, the velocity of the field never becomes large enough to ignite particle production, and the oscillations are damped only by cosmic expansion. Similarly to the QCD axion and other generic axion-like particles, during the oscillatory phase, the relaxion will contribute to the energy density of the universe as a cold dark matter component. The abundance at the onset of the oscillatory phase is given by [65]

$$Y_{\text{mis}}^\phi = \frac{1}{m_\phi} \frac{\rho_\phi}{s} = \frac{m_\phi \phi_i^2 / 2}{2\pi^2 g_* T_{\text{osc}}^3 / 45} \quad (6.1)$$

where ϕ_i is defined as the displacement from the minimum of the periodic potential in which the field has been trapped and T_{osc} is the temperature when oscillations start as the Hubble rate drops below the value of the thermal mass: $m_a(T_{\text{osc}}) = 3H(T_{\text{osc}})$. In our case, the maximum temperature of the plasma is $T_{\text{pp}} \sim \Lambda$, that is lower than the value set by the overdamping of the oscillations except for very low masses, as shown in Fig. 13. In most of our parameter space we can therefore assume an initial temperature $T_{\text{osc}} = T_{\text{pp}} \sim \Lambda$, up to the numerical factors of Eq. 4.11.

The initial amplitude of the oscillations ϕ_i can be simply estimated as follows. In the initial stage of oscillations, if the amplitude is large, particle production will

efficiently damp it down until the velocity of the field ϕ is too low to induce the tachyonic growth. This happens when $\dot{\phi}_c \sim 2m_Z f$ (see Eq. (3.18)), where the mass of the gauge boson is now given by the measured value $m_Z \approx 90$ GeV. From this moment ϕ will oscillate freely, with an initial amplitude which is obtained by using energy conservation:

$$\Delta V \approx \frac{1}{2} \frac{\Lambda_b^4}{f'^2} \phi_i^2 = \frac{1}{2} \dot{\phi}_c^2 \lesssim 2f^2 m_Z^2 \implies \phi_i \lesssim 2 \frac{f' f m_Z}{\Lambda_b^2}. \quad (6.2)$$

Using Eq. (4.3), $f \sim \Lambda^2/(2v_{\text{EW}})$, gives

$$\phi_i \lesssim \frac{\Lambda^2}{\Lambda_b^2} \frac{m_Z}{v_{\text{EW}}} f'. \quad (6.3)$$

A similar bound is obtained by requiring that $\phi_i \lesssim \pi f'$. The two conditions are numerically similar in the region where Λ and Λ_b are of the same order. In the bounds presented below, ϕ_i is chosen to saturate the minimum of these two conditions, the obtained bound is the most stringent one, and it can be alleviated by considering smaller values of ϕ_i . Anyhow, from (6.3), we deduce that Y_{mis}^ϕ is bounded by f'/Λ and can therefore be very large and dangerous.

6.1.2 Thermal production

A hot population of ϕ particles is produced via the process $Z/\gamma + q/\ell \rightarrow \phi + q/\ell$. This is mediated by the $\phi F\tilde{F}$ coupling, analogously to the standard QCD axion coupled to photons, and the role of the photon is played by the massless hypercharge gauge boson. The abundance due to this process is given by [65]

$$Y_{\text{th}}^\phi = Y_{\text{eq}} \left[1 - \exp \left(- \int_1^x \frac{\Gamma}{x' H} dx' \right) \right], \quad (6.4)$$

where $x = T_{\text{pp}}/T$, $Y_{\text{eq}} = 45\zeta(3)/(2\pi^4 g_*^S)$ is the equilibrium abundance, and Γ is the interaction rate [66]

$$\Gamma = \frac{1}{9\pi} g_1^6 (2 \log(3/g_1) + 0.82) \frac{T^3}{f'^2}. \quad (6.5)$$

Depending on whether m_ϕ is smaller or larger than the EW scale, the integral above has a natural cutoff at $T \sim v_{\text{EW}}$ or $T \sim m_\phi$, respectively. In the first case, in the broken electroweak phase, the rate Γ is suppressed by powers of T/m_Z , while in the second case, at $T \lesssim m_\phi$ the relaxion is too heavy to be produced by the interactions of light particles. We checked numerically that, in our parameter space, the integral is always large enough to suppress the negative exponential, resulting in a final abundance at freeze-in equal to the thermal value Y_{eq} .

In addition to the process considered above, the relaxion can also be thermally produced in processes involving the ϕgg and $\phi \bar{q}q$ couplings that are obtained through the relaxion–Higgs mixing [34]. In our case, the insertion of the mixing angle makes this contribution negligible.

Except in the low Λ_b region in scenario E, the misalignment contribution Y_{mis}^ϕ dominates over the thermal contribution Y_{th}^ϕ .

6.2 Dark matter relic abundance

If the relaxion is stable on cosmological timescales, its relic abundance can contribute to the present dark matter density, and must therefore not exceed the measured value of $\Omega_{\text{cdm}}h^2 \simeq 0.12$. The present abundance is given by

$$\Omega_\phi = \frac{s_0 m_\phi}{\rho_{\text{crit}}} Y_\phi, \quad (6.6)$$

where $\rho_{\text{crit}} \approx 4 \times 10^{-47} \text{ GeV}^4$ is the critical density of the universe and $s_0 \approx 2 \times 10^{-38} \text{ GeV}^3$ is the present entropy density. In the region of m_ϕ where the relaxion is cosmologically stable, its relic abundance is too large in our model. The corresponding exclusion is shown in Fig. 14, and covers all the parameter space in which the relaxion is stable on cosmological timescales. Unfortunately, the relaxion is therefore not a viable dark matter candidate.

6.3 Primordial abundances of light elements

Relaxions decaying after the Big Bang Nucleosynthesis (BBN) epoch are strongly constrained by bounds on the primordial abundances of light elements. A long-lived unstable particle which decays into electromagnetic or hadronic particles can affect the light element abundances by photodissociation, hadrodissociation, and $p \leftrightarrow n$ conversion processes [67]. In our case, the decaying particle dominates the energy density, thus heavily affecting neutrino thermalisation, which constrains the decay to happen well before the BBN. Therefore, the abundance of light elements exclude the scenario where the relaxion decays after $\tau_\phi \lesssim 2 \times 10^{-2} \text{ s}$ [68]. The excluded region is shown in orange in Fig. 14.

Even later decays, occurring close to the time of CMB emission, or reionization, will constrain parameter space that is already ruled out by BBN bounds. Anyhow, we report them for completeness in the remaining of Section 6.

6.4 CMB distortions

The decay of the relaxion can inject energy in the CMB, modifying its spectral properties. If this happens before $z \sim 2 \times 10^6$ this has no effect since thermalisation is still efficient. At a redshift of $z \sim 2 \times 10^6$, corresponding to a time of 10^6 s , the number-changing double Compton scattering process $\gamma + e \rightarrow \gamma + \gamma + e$ decouples, and if photons are injected after this point the Planck distribution, in which the particle number is fixed by the total energy, cannot be restored. Thermal equilibrium is maintained through the Compton scattering $\gamma + e \rightarrow \gamma + e$, but the distribution is of a Bose-Einstein one, with non vanishing chemical potential μ . This type of distortion is called μ -distortion, and is constrained by the COBE/FIRAS data to be very small: $|\mu| \lesssim 0.9 \times 10^{-4}$ [69] (see also [34, 66]). This excludes the region where the relaxion is unstable and $\delta = \rho_\phi/\rho_\gamma > 1$, which is the case in our scenario. As a consequence, lifetimes larger than 10^6 s and shorter than the age of the universe are excluded by CMB distortions, as shown with an horizontal hashing in Fig. 14.

A similar reasoning can be applied to lifetimes larger than $\sim 10^9$ s, when the relaxion decays after the decoupling of the Compton scattering such that kinetic equilibrium between electrons and photons cannot be maintained anymore. This generates deviations of the CMB spectrum from a Bose-Einstein distribution named y -distortions [34, 66]. Again, in our model $\delta > 1$ in this region, which is thus excluded (vertical hashing in Fig. 14).

6.5 Entropy injection before CMB formation

If the relaxion decays after neutrino decoupling ($t \sim 1$ s) and before Big Bang nucleosynthesis ($t \sim 3$ min), it can reduce the effective number of neutrino species N_{eff} which in the SM is predicted to be 3.046 and is bounded to be larger than 2.6 [70]. On the other hand, if ϕ decays after BBN but before CMB formation, the baryon asymmetry η_B would be diluted between the two, while data from BBN and CMB show good agreement within the experimental uncertainties.

The relevant quantity is the entropy injection after the relaxion decay. We checked numerically that, for $1\text{ s} \lesssim \tau_\phi \lesssim 3.8 \times 10^5$ years, the relaxion is sufficiently heavy to become non relativistic before decaying. In this case, the entropy injection is [65]:

$$\frac{\Delta S}{S} = x \langle (g_*^S)^{1/3} \rangle^{3/4} m_\phi Y_\phi \sqrt{\frac{\tau_\phi}{M_{\text{Pl}}}} \quad (6.7)$$

where g_*^S must be appropriately averaged over the decay process and x is a $O(1)$ factor estimated as 1.5 – 1.83 depending on whether or not ϕ dominates the energy density before decaying [65, 71]. For simplicity, we considered the maximum values of these quantities, but given the power scaling, the difference is negligible for our purposes. The variation in the number of neutrino species due to the entropy injection is

$$N_{\text{eff}} = 3.046 \left(1 + \frac{\Delta S}{S} \right)^{-4/3} \Rightarrow \frac{\Delta S}{S} \lesssim 0.13. \quad (6.8)$$

Similarly, the dilution of the baryon asymmetry is given by

$$\frac{\eta_{\text{after}}}{\eta_{\text{before}}} = \left(1 + \frac{\Delta S}{S} \right)^{-1}. \quad (6.9)$$

A limit $\Delta S/S \lesssim 2\%$ can be naively estimated from the size of the uncertainty band in the CMB measurement [72]. Among these bounds, the only relevant one comes from the non variation of η_B between BBN and CMB. The results are reported in Fig. 14 for scenarios B-E. No bound can be derived in scenario A.

6.6 Reionization

Photons produced in the relaxion decays during reionization between $z \sim 100$ and $z \sim 6$, will tend to ionize the universe with a rather soft redshift dependence $\propto (1+z)^{-3/2}$ [66], which is not favoured by data. Given the large predicted abundance of ϕ in this range of lifetimes, this observation excludes a relaxion with a lifetime of $\sim 10^{14} - 10^{16}$ s. We also report this constraint in Fig. 14.

6.7 Overview

The combination of constraints is shown in Fig. 14. In the region where the relaxion is unstable, the strongest bound comes from primordial abundances of light elements, which is shown in orange in Fig. 14. In our scenario, the relaxion relic abundance is too large, so the quantity $m_\phi Y_\phi$ is always above the current bound in the region of the parameter space where the relaxion decays between $\tau_\phi \sim 10^{-2} s$ and $\tau_\phi \sim 10^{17} s$. The bounds from CMB distortions, reionization, and entropy injection are also shown in Fig. 14. In the region the relaxion is cosmologically stable, it is over-abundant. This corresponds to the exclusion region in blue in Fig. 14.

Taking into account all the constraints in this section, the allowed mass ranges for our five benchmarks are approximately given by

$$\begin{aligned} \text{scenario A: } & m_\phi \in [m_Z, 10 \text{ TeV}] \\ \text{scenario B: } & m_\phi \in [300 \text{ MeV}, 10 \text{ TeV}] \\ \text{scenario C: } & m_\phi \in [m_Z, 30 \text{ TeV}] \\ \text{scenario D: } & m_\phi \in [m_Z, 100 \text{ TeV}] \\ \text{scenario E: } & m_\phi \in [3.8 \text{ GeV}, 700 \text{ TeV}] \end{aligned} \quad (6.10)$$

Comparing with the resulting mass ranges above with the ones in (5.3), we see that all the lower bounds are shifted to higher masses, except the scenario B. In this case, in the mass range accessible to our model (see Fig. 12), the relaxion decays before the BBN epoch so it is not constrained by the primordial abundances of light elements. Astrophysical probes (SN1987a supernova, global-cluster star bounds, CAST) cannot constrain our scenario as their limits apply to relaxion masses below the lower bounds in (6.10), see e.g. [34].

Another crucial difference between our case and the standard relaxion scenario is the relaxion relic abundance. When the scanning happens during inflation and the stopping mechanism is given by a Higgs-dependent barrier, the dominant contribution to the relaxion abundance is the thermal production [2, 34]. On the other hand, in the scenario presented here, the misalignment contribution is the dominant one. There are two main reasons for this difference. First, in our case, the initial misalignment angle is set by time when particle production becomes inefficient and ϕ can oscillate freely. In the usual case, relaxation happens during inflation then quantum fluctuations generate a spreading of the field around the classical value. The initial misalignment angle is then determined by the maximum spread displacement at the end of inflation [2, 34]. Second, the temperature when the relaxion starts the oscillations, which determines when its energy density starts to redshift as matter, is lower than the value set by the overdamping of the oscillations (given by $m_a(T_{\text{osc}}) \approx 3H(T_{\text{osc}})$) in most of our parameter space, see Fig. 13. The later the field starts to oscillate and dilute its energy density, the larger is the misalignment contribution.

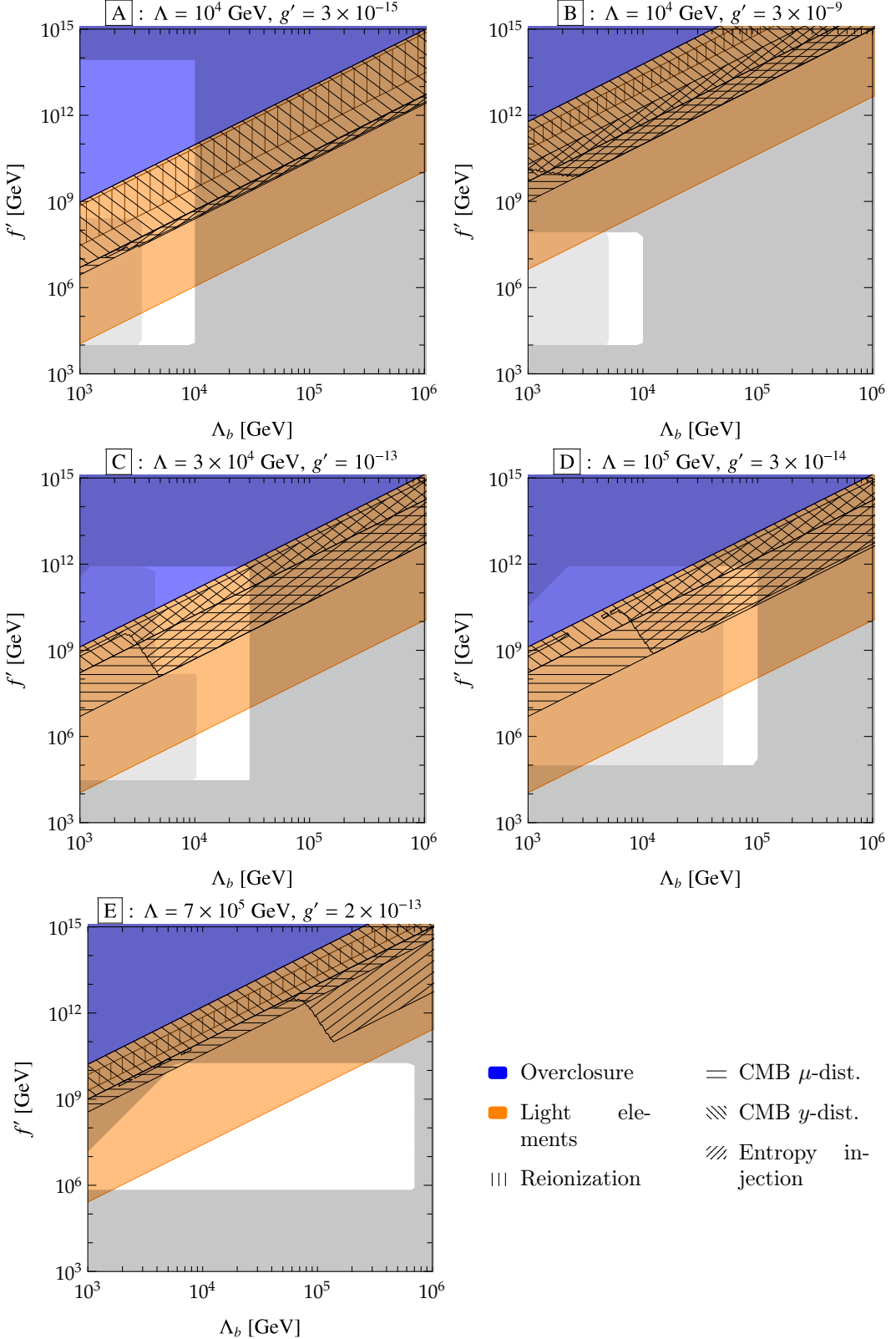


Figure 14. Combination of all the cosmological constraints for each of the five benchmark points in the plane $[\Lambda_b, f']$ defined in Eq. (4.26) and shown in red in Figure 7. The white region denotes the allowed region. To be compared with Figure 8.

7 Summary and Conclusions

In summary, we have investigated in detail the viability of the cosmological relaxation mechanism of the electroweak scale taking place after inflation [10], and starting in a universe dominated by radiation. In this case, the friction needed to stop and prevent the relaxion from running away down its potential, comes from particle production instead of exponential Hubble expansion. We showed that Higgs particle production cannot be used for this purpose. Instead, particle production is sourced by a relaxion coupling to a $U(1)$ electroweak gauge field of the type

$$-\frac{\phi}{4f} \left(g_2^2 W \widetilde{W} - g_1^2 B \widetilde{B} \right) \quad (7.1)$$

where g_1 and g_2 are respectively the couplings for $U(1)_Y$ and $SU(2)_W$. This particular combination is crucial since it does not contain the photon. It arises naturally in some UV completions, for instance PNGBs may inherit such anomalous coupling structure.

Such coupling induces exponential particle production only when the Higgs VEV approaches zero and the $U(1)$ gauge field (7.1) becomes nearly massless. Particle production comes at the expense of kinetic energy of the relaxion. Being slowed down, it can no longer overcome the large (Higgs-independent) barriers. This stops very efficiently the relaxion when the Higgs mass parameter approaches its critical value from above, as illustrated in Fig. 15. In this realisation of the relaxion mechanism, the universe starts in the broken electroweak phase, with a Higgs VEV of the order of the cutoff scale Λ . The universe is initially reheated in a hidden sector, such that the Standard Model is not thermalised and the Higgs potential receives negligible thermal corrections. This is the only non-trivial assumption for a successful implementation of this scenario. Reheating of the Standard Model sector takes place at the end of the relaxation mechanism and is induced by the same relaxion coupling (7.1) which is responsible for the stopping mechanism through gauge boson production. As the relaxion potential energy is transferred to the Standard Model thermal bath, the reheat temperature is expected to be close to the cutoff scale Λ . Interestingly, the more minimal scenario in which the Standard Model is reheated just after inflation and the relaxation phase starts after the temperature has been redshifted below the scale Λ , is constrained but still viable, see Fig. 3.

The relaxion initial velocity can be obtained either from a coupling with the hidden sector or through an interaction with the inflation sector. For instance, a coupling of the relaxion to the inflaton can provide an effective slope, which results in a large initial velocity.

We determined the parameter space in which such mechanism works and satisfies all cosmological constraints. Free parameters are the cutoff scale Λ , the Higgs-relaxion coupling g' , the height of the barriers Λ_b and the frequency of the periodic potential f' . Our results are summarised in Figure 7 and 14. Fig. 7 shows the allowed region in the plane $[g', \Lambda]$ while Fig. 14 shows the open region in the plane $[f', \Lambda_b]$ for the five benchmark points of Fig. 14. The cutoff scale Λ can be as large as ~ 100 TeV, and may be pushed to 10^6 TeV under less conservative assumptions on the thermalisation

process. Large couplings $g' \gtrsim 10^{-3}$ are incompatible with the condition that the Higgs field tracks the minimum of its potential during the cosmological evolution. This condition is absent in the relaxion proposal relying on inflation and Higgs-dependent barriers, although an effectively comparable condition comes from preventing large quantum corrections induced by the coupling generating the Higgs-dependent barrier. Coupling values smaller than 10^{-16} are forbidden in our framework as they would lead to slow-rolling of the relaxion and therefore inflation induced by the relaxion field. In comparison, the relaxion-associated-with-inflation proposal typically has couplings which are smaller by many orders of magnitude (see comparison in right plot of Fig. 7), and are only bounded by the condition that quantum displacements of the relaxion do not dominate its classical motion.

This mechanism is very difficult to test experimentally, despite the relatively low cutoff scale and rather large g' values that we are pointing to, as the relaxion manifests itself either via its mixing with the Higgs or via its coupling to the Z and W gauge bosons through (7.1). We estimated that future colliders such as the FCC-pp can probe the relaxion only if Λ is below 5 TeV, while SHiP may probe it for Λ below ~ 10 TeV. The relaxion is heavy compared to the original relaxion proposal. Its mass ranges values from 0.1 GeV up to Λ . It necessarily decays before BBN. It cannot be cosmologically stable, as otherwise it would overclose the universe. Thus the relaxion cannot be dark matter in this scenario.

One further step to probe this mechanism will be to determine in more detail cosmological implications of the stopping mechanism, which involves out-of-equilibrium conditions that may lead to observable imprints. The reheating process in itself deserves further investigation. The coupling (7.1) has been used in the context of inflation as a source of gravitational waves, CMB non-gaussianities or magnetogenesis, and its effects in the context of the lower scale relaxion mechanism should be studied.

Another important insight will come from understanding how the baryon asymmetry can be explained in this set up. Baryogenesis cannot take place before relaxation as it would be diluted away by the entropy injection during reheating coming from the relaxion decay. As the philosophy of the relaxion mechanism is that no new physics occurs at the EW scale, we expect the EW phase transition that occurs after reheating and EW symmetry restoration to be standard-like. This forbids the possibility of standard EW baryogenesis as the requirement of a first-order EW phase transition typically requires an additional weak scale scalar field. An alternative baryogenesis mechanism has to be found. For concrete progress to be made in this direction, the determination of the reheat temperature is required, and this work strongly motivates such a dedicated study.

In conclusion, cosmological relaxation of the EW scale rather independently from inflation is a viable option that opens interesting opportunities and deserves further investigation.

Acknowledgments

We would like to thank Francesco Cicciarella, Mafalda Dias, Jonathan Frazer, David E. Kaplan, Kazunori Kohri, Gustavo Marques-Tavares, Mauro Pieroni, Antonio Riotto, Lorenzo Ubaldi, Augustin Vanrietvelde, and Sebastian Wild for useful discussions. In particular, we are grateful to Oleksii Matsedonskyi and Alexander Westphal for discussions regarding the initial conditions and to Valerie Domcke for innumerable discussions and comments. NF and EM thank the organizers and participants of the Cosmological probes of BSM Workshop in Benasque for interesting discussions during the completion of this work.

A Equations of Motion

A.1 Higgs case

Here we consider the equations of motions for the model given in Eq. (2.1), the Higgs field h is decomposed as a classical field and quantum fluctuation,

$$h = h_0 + \chi. \quad (\text{A.1})$$

The χ field can be expanded in Fourier modes as

$$\chi(t, \vec{x}) = \int \frac{d^3 k}{(2\pi)^{3/2}} \left(a_{\vec{k}} \chi_{\vec{k}}(t) e^{i\vec{k} \cdot \vec{x}} + a_{\vec{k}}^\dagger \chi_{\vec{k}}^*(t) e^{-i\vec{k} \cdot \vec{x}} \right), \quad (\text{A.2})$$

where the creation and annihilation operator $a_{\vec{k}}^\dagger, a_{\vec{k}}$ satisfy the usual commutation relations

$$[a_{\vec{k}}, a_{\vec{k}'}] = [a_{\vec{k}}^\dagger, a_{\vec{k}'}^\dagger] = 0, \quad [a_{\vec{k}}, a_{\vec{k}'}^\dagger] = (2\pi)^3 \delta^3(\vec{k} - \vec{k}'), \quad (\text{A.3})$$

and the normalized χ_k wave functions satisfy

$$\dot{\chi}_{\vec{k}}^* \chi_{\vec{k}} - \chi_{\vec{k}}^* \dot{\chi}_{\vec{k}} = i. \quad (\text{A.4})$$

As in our scenario the relaxation dynamics happens after inflation, for simplicity, here we consider flat space so the equations of motion can be written as

$$\ddot{\phi} - g\Lambda^3 + \frac{1}{2}g'\Lambda h_0^2 + \frac{1}{2}g'\Lambda \int \frac{d^3 k}{(2\pi)^3} \left(|\chi_{\vec{k}}|^2 - \frac{1}{2\omega_k} \right) + \frac{\Lambda_b^4}{f'} \sin \left(\frac{\phi}{f'} \right) = 0 \quad (\text{A.5})$$

$$\ddot{h} + \left[g'\Lambda\phi - \Lambda^2 + 3\lambda \int \frac{d^3 k}{(2\pi)^3} \left(|\chi_{\vec{k}}|^2 - \frac{1}{2\omega_k} \right) \right] h_0 + \lambda h_0^3 = 0 \quad (\text{A.6})$$

$$(\partial^2 + k^2 + g'\Lambda\phi - \Lambda^2 + 3\lambda h_0^2) \chi_{\vec{k}} = 0, \quad (\text{A.7})$$

where $\omega_k = \sqrt{k^2 + (g'\phi\Lambda - \Lambda^2 + 3\lambda h_0^2)}$ is the frequency of the quantum field $\chi_{\vec{k}}$, with $k^2 \equiv \vec{k} \cdot \vec{k}$. Note that we consider the linearized equation of motion for $\chi_{\vec{k}}$ as higher order terms are sub-dominant. The subtraction in the parentheses in Eqs. (A.5) and (A.6) refers to the first order WKB mode functions $\chi_{\vec{k}}^{\text{WKB}} = \exp(i\omega_k)/\sqrt{2\omega_k}$, which is needed to cancel a divergence in the effective potential (see e.g. [44, 73]). In addition, we assume that the relaxion field is homogeneous in space, i.e. $\phi(t, \vec{x}) = \phi(t)$.

A.2 Gauge bosons case

The aim of this appendix is to derive equations (3.11), (3.12), (3.13) and (3.16) and display numerical solutions. We start from the gauge invariant Lagrangian

$$\mathcal{L} = -\frac{1}{4}F_{\mu\nu}F^{\mu\nu} + \frac{1}{2}\partial_\mu\phi\partial^\mu\phi + (D_\mu\Phi_H)^\dagger D^\mu\Phi_H - \frac{\phi}{4f}\epsilon^{\mu\nu\rho\sigma}F_{\mu\nu}F_{\rho\sigma} - V(\phi, \Phi_H^\dagger\Phi_H) \quad (\text{A.8})$$

where Φ_H is the Higgs doublet and the potential $V(\phi, \Phi_H^\dagger\Phi_H)$ is given in Eq. (2.1). After gauge symmetry breaking, the Goldstone bosons can be reabsorbed in the field V_μ , and the Lagrangian reads

$$\mathcal{L} = -\frac{1}{4}F_{\mu\nu}F^{\mu\nu} - \frac{1}{2}\partial_\mu\phi\partial^\mu\phi + \frac{1}{2}\partial_\mu h\partial^\mu h + \frac{1}{2}g_V^2 h^2 V_\mu V^\mu - \frac{\phi}{4f}\epsilon^{\mu\nu\rho\sigma}F_{\mu\nu}F_{\rho\sigma} - V(\phi, h). \quad (\text{A.9})$$

The equations of motion for the h and for ϕ fields are trivial:

$$\square\phi + \frac{\partial V(\phi, h)}{\partial\phi} - \frac{1}{4f}F\tilde{F} = 0 \quad (\text{A.10})$$

$$\square h + \frac{\partial V(\phi, h)}{\partial h} - g_V^2 V_\mu V^\mu h = 0 \quad (\text{A.11})$$

For the field V_μ we get instead

$$\square V^\mu - \partial^\mu\partial_\nu V^\nu - 2\epsilon^{\alpha\beta\gamma\mu}\frac{\partial_\gamma\phi}{f}\partial_\alpha V_\beta + g_V^2 h^2 V^\mu = 0. \quad (\text{A.12})$$

If we take the divergence of this relation we obtain

$$\partial_\mu(h^2 V^\mu) = 0, \quad \text{i.e.} \quad \partial_\mu V^\mu = -2\frac{\partial_\mu h}{h}V^\mu \quad (\text{A.13})$$

which shows that the usual assumption $\partial_\mu V^\mu = 0$ is not consistent in this case.

Assuming for simplicity that the fields ϕ and h are spatially uniform, the equations of motion simplify to

$$\begin{cases} \ddot{\phi} + \frac{\partial V(\phi, h)}{\partial\phi} - \frac{1}{4f}F\tilde{F} = 0 \\ \ddot{h} + \frac{\partial V(\phi, h)}{\partial h} - g_V^2 V_\mu V^\mu h = 0 \\ \ddot{V}^j + \partial_i\partial^i V^j + 2\partial^j\frac{\dot{h}}{h}V^0 - 2\epsilon^{jkl}\frac{\dot{\phi}}{f}\partial_k V_l + g_V^2 h^2 V^j = 0 \\ (\partial_i\partial^i + g_V^2 h^2)V^0 - \partial_i\dot{V}^i = 0 \end{cases} \quad (\text{A.14})$$

The first two equations in (A.14) reproduce the equations (3.11) and (3.12). After a Fourier transform, the equation for the V^0 component becomes a simple algebraic

equation, and V_0 can be expressed in terms of the other components. Projecting the spatial part onto helicity components we obtain

$$\begin{cases} \ddot{V}_\pm + (k^2 + g_V^2 h^2) V_\pm \pm \frac{\dot{\phi}}{f} k V_\pm = 0 \\ \ddot{V}_L + 2 \frac{\dot{h}}{h} \frac{k^2}{k^2 + g_V^2 h^2} \dot{V}_L + (k^2 + g_V^2 h^2) V_L = 0 \\ V_0 = -i \frac{k \dot{V}_L}{k^2 + g_V^2 h^2} \end{cases} \quad (\text{A.15})$$

The first equation above reproduces (3.13).

The terms $F_{\mu\nu} \tilde{F}^{\mu\nu}$ and $V_\mu V^\mu$ in the equations of motion for ϕ and h must be interpreted as the expectation values of the quantum operators on the in-vacuum state. Introducing the creation and annihilation operators we write

$$V_\mu(t, \vec{x}) = \int \frac{d^3 k}{(2\pi)^3} \sum_\lambda V_\mu^{(\lambda)}(t, \vec{k}) e^{i\vec{k} \cdot \vec{x}} \left(a_\vec{k}^\lambda + (a_{-\vec{k}}^\lambda)^\dagger \right) \quad (\text{A.16})$$

where $V_\mu^{(\lambda)}(t, -\vec{k}) = V_\mu^{(\lambda)}(t, \vec{k})^*$ for the reality of the $V_\mu(t, \vec{x})$ field, and the creation/annihilation operators satisfy the usual commutation relations

$$[a_\vec{k}^\lambda, a_{\vec{k}'}^{\lambda'}] = (2\pi)^3 \delta^{\lambda\lambda'} \delta^3(\vec{k} - \vec{k}'), \quad [a, a] = [a^\dagger, a^\dagger] = 0. \quad (\text{A.17})$$

With this we get

$$\begin{aligned} \langle V_\mu V^\mu \rangle &= \int \frac{d^3 k}{(2\pi)^3} \sum_\lambda (|V_0|^2 - |V_+|^2 - |V_-|^2 - |V_L|^2) \\ &\approx - \int \frac{d^3 k}{(2\pi)^3} \sum_\lambda (|V_+|^2 + |V_-|^2) . \end{aligned} \quad (\text{A.18})$$

where in the last line we have neglected the contribution of the longitudinal and time-like components. Similarly, for $F \tilde{F}$ we get

$$\frac{1}{4} \langle F \tilde{F} \rangle = \langle \epsilon^{\mu\nu\rho\sigma} \partial_\mu V_\nu \partial_\rho V_\sigma \rangle = \int \frac{d^3 k}{(2\pi)^3} k \frac{\partial}{\partial t} (|V_+|^2 - |V_-|^2) . \quad (\text{A.19})$$

which is equation (3.16). Equations (A.18) and (A.19) must be renormalized by subtracting the same quantities computed on the first order WKB mode functions $V_\pm^{\text{WKB}} = \exp(i\omega_{k\pm})/\sqrt{2\omega_{k\pm}}$. In Fig. 15, we show numerical solutions of these equations, as commented in Section 3.2.

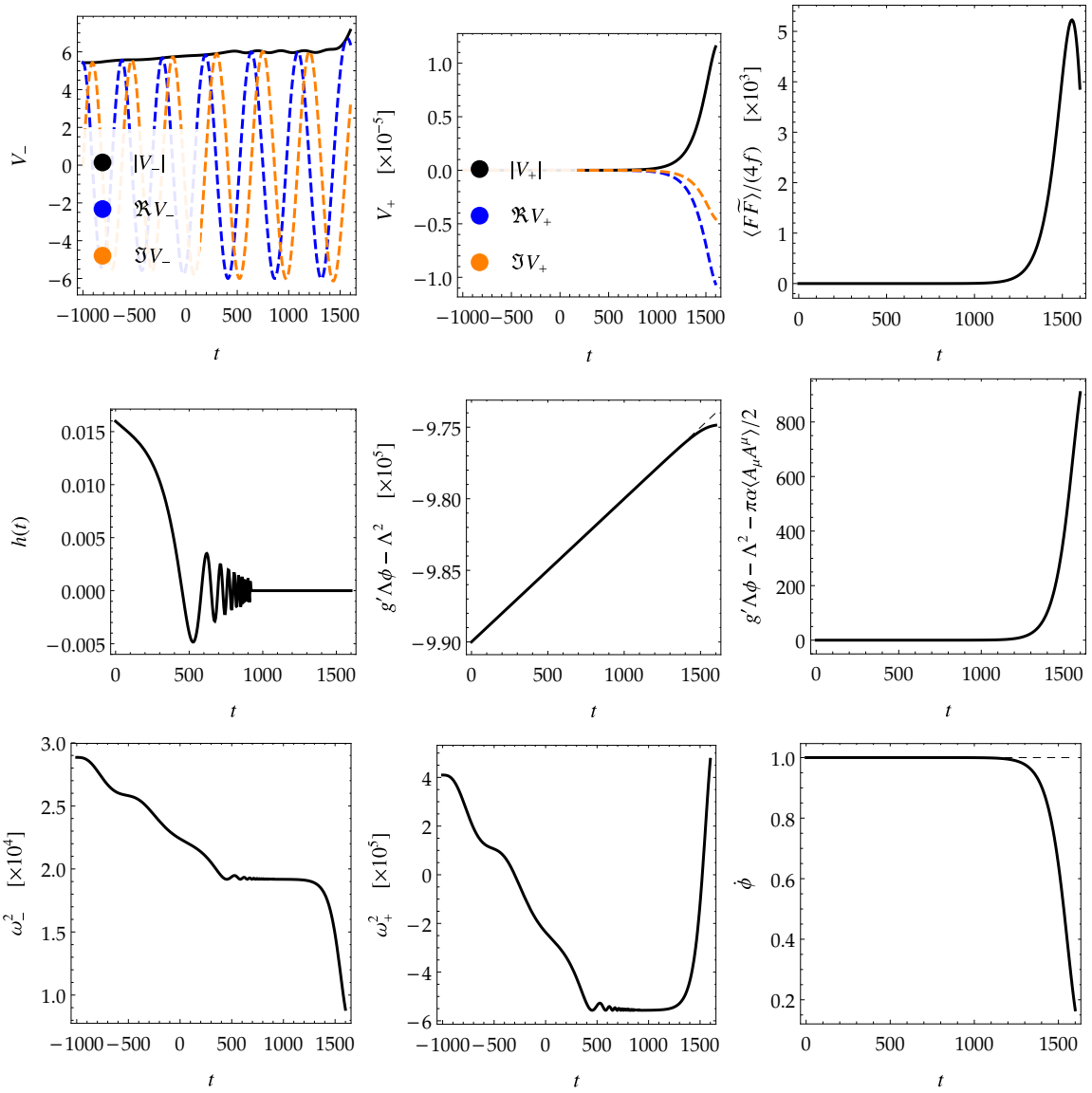


Figure 15. Solutions of the system of equations (3.11, 3.12, 3.13) (which does not include thermalisation effects). While time scales will be different, we expect similar qualitative features when the effect of temperature is taken into account. All quantities are expressed in units of Λ . The top panel shows that the transverse polarisation V_- does not feature any tachyonic instability and is nearly constant, while the other transverse polarization V_+ exhibits a tachyonic growth. The operator $\langle F\tilde{F} \rangle$ grows accordingly. The relaxion velocity $\dot{\phi}$ drops. The Higgs mass parameter $g'\Lambda\phi - \Lambda^2$ stabilises. The contribution to the Higgs mass parameter from the gauge field quickly grows and restores the EW symmetry. The Higgs vev stabilizes to a vanishing value (and, for simplicity, we set it to zero after a few oscillations). The left plot of the bottom panel shows that the time when the frequency squared of one of the modes ω_+^2 becomes negative coincides with gauge field particle production.

References

- [1] P. W. Graham, D. E. Kaplan and S. Rajendran, *Cosmological Relaxation of the Electroweak Scale*, *Phys. Rev. Lett.* **115** (2015) 221801, [[1504.07551](#)].
- [2] J. R. Espinosa, C. Grojean, G. Panico, A. Pomarol, O. Pujolàs and G. Servant, *Cosmological Higgs-Axion Interplay for a Naturally Small Electroweak Scale*, [1506.09217](#).
- [3] R. S. Gupta, Z. Komargodski, G. Perez and L. Ubaldi, *Is the Relaxion an Axion?*, *JHEP* **02** (2016) 166, [[1509.00047](#)].
- [4] S. Abel and R. J. Stewart, *Shift-Symmetries at Higher Order*, *JHEP* **02** (2016) 182, [[1511.02880](#)].
- [5] K. Choi and H. Kim, *Aligned natural inflation with modulations*, *Phys. Lett.* **B759** (2016) 520–527, [[1511.07201](#)].
- [6] L. E. Ibáñez, M. Montero, A. Uranga and I. Valenzuela, *Relaxion Monodromy and the Weak Gravity Conjecture*, *JHEP* **04** (2016) 020, [[1512.00025](#)].
- [7] A. Hebecker, F. Rompineve and A. Westphal, *Axion Monodromy and the Weak Gravity Conjecture*, *JHEP* **04** (2016) 157, [[1512.03768](#)].
- [8] L. McAllister, P. Schwaller, G. Servant, J. Stout and A. Westphal, *Runaway Relaxion Monodromy*, *JHEP* **02** (2018) 124, [[1610.05320](#)].
- [9] E. Hardy, *Electroweak relaxation from finite temperature*, *JHEP* **11** (2015) 077, [[1507.07525](#)].
- [10] A. Hook and G. Marques-Tavares, *Relaxation from particle production*, *JHEP* **12** (2016) 101, [[1607.01786](#)].
- [11] S. P. Patil and P. Schwaller, *Relaxing the Electroweak Scale: the Role of Broken dS Symmetry*, *JHEP* **02** (2016) 077, [[1507.08649](#)].
- [12] J. Jaeckel, V. M. Mehta and L. T. Witkowski, *Musings on cosmological relaxation and the hierarchy problem*, *Phys. Rev.* **D93** (2016) 063522, [[1508.03321](#)].
- [13] L. Marzola and M. Raidal, *Natural relaxation*, *Mod. Phys. Lett.* **A31** (2016) 1650215, [[1510.00710](#)].
- [14] S. Di Chiara, K. Kannike, L. Marzola, A. Racioppi, M. Raidal and C. Spethmann, *Relaxion Cosmology and the Price of Fine-Tuning*, *Phys. Rev.* **D93** (2016) 103527, [[1511.02858](#)].
- [15] J. L. Evans, T. Gherghetta, N. Nagata and M. Peloso, *Low-scale D-term inflation and the relaxion mechanism*, *Phys. Rev.* **D95** (2017) 115027, [[1704.03695](#)].
- [16] W. Tangarife, K. Tobioka, L. Ubaldi and T. Volansky, *Relaxed Inflation*, [1706.00438](#).
- [17] W. Tangarife, K. Tobioka, L. Ubaldi and T. Volansky, *Dynamics of Relaxed Inflation*, *JHEP* **02** (2018) 084, [[1706.03072](#)].
- [18] K. Choi, H. Kim and T. Sekiguchi, *Dynamics of the cosmological relaxation after reheating*, *Phys. Rev.* **D95** (2017) 075008, [[1611.08569](#)].
- [19] B. Batell, G. F. Giudice and M. McCullough, *Natural Heavy Supersymmetry*, *JHEP* **12** (2015) 162, [[1509.00834](#)].

[20] J. L. Evans, T. Gherghetta, N. Nagata and Z. Thomas, *Naturalizing Supersymmetry with a Two-Field Relaxion Mechanism*, *JHEP* **09** (2016) 150, [[1602.04812](#)].

[21] B. Batell, M. A. Fedderke and L.-T. Wang, *Relaxation of the Composite Higgs Little Hierarchy*, *JHEP* **12** (2017) 139, [[1705.09666](#)].

[22] O. Antipin and M. Redi, *The Half-composite Two Higgs Doublet Model and the Relaxion*, *JHEP* **12** (2015) 031, [[1508.01112](#)].

[23] A. Agugliaro, O. Antipin, D. Becciolini, S. De Curtis and M. Redi, *UV complete composite Higgs models*, *Phys. Rev.* **D95** (2017) 035019, [[1609.07122](#)].

[24] Z. Lalak and A. Markiewicz, *Dynamical relaxation in 2HDM models*, *J. Phys.* **G45** (2018) 035002, [[1612.09128](#)].

[25] O. Matsedonskyi, *Mirror Cosmological Relaxation of the Electroweak Scale*, *JHEP* **01** (2016) 063, [[1509.03583](#)].

[26] O. Davidi, R. S. Gupta, G. Perez, D. Redigolo and A. Shalit, *The Nelson-Barr Relaxion*, [1711.00858](#).

[27] K. Choi and S. H. Im, *Realizing the relaxion from multiple axions and its UV completion with high scale supersymmetry*, *JHEP* **01** (2016) 149, [[1511.00132](#)].

[28] D. E. Kaplan and R. Rattazzi, *Large field excursions and approximate discrete symmetries from a clockwork axion*, *Phys. Rev.* **D93** (2016) 085007, [[1511.01827](#)].

[29] G. F. Giudice and M. McCullough, *A Clockwork Theory*, *JHEP* **02** (2017) 036, [[1610.07962](#)].

[30] N. Fonseca, B. Von Harling, L. De Lima and C. S. Machado, *A warped relaxion*, [1712.07635](#).

[31] N. Fonseca, L. de Lima, C. S. Machado and R. D. Matheus, *Large field excursions from a few site relaxion model*, *Phys. Rev.* **D94** (2016) 015010, [[1601.07183](#)].

[32] T. Kobayashi, O. Seto, T. Shimomura and Y. Urakawa, *Relaxion window*, *Mod. Phys. Lett.* **A32** (2017) 1750142, [[1605.06908](#)].

[33] K. Choi and S. H. Im, *Constraints on Relaxion Windows*, *JHEP* **12** (2016) 093, [[1610.00680](#)].

[34] T. Flacke, C. Frugiuele, E. Fuchs, R. S. Gupta and G. Perez, *Phenomenology of relaxion-Higgs mixing*, *JHEP* **06** (2017) 050, [[1610.02025](#)].

[35] H. Beauchesne, E. Bertuzzo and G. Grilli di Cortona, *Constraints on the relaxion mechanism with strongly interacting vector-fermions*, *JHEP* **08** (2017) 093, [[1705.06325](#)].

[36] F. P. Huang, Y. Cai, H. Li and X. Zhang, *A possible interpretation of the Higgs mass by the cosmological attractive relaxion*, *Chin. Phys.* **C40** (2016) 113103, [[1605.03120](#)].

[37] O. Matsedonskyi and M. Montull, *Light Higgs from Pole Attractor*, [1709.09090](#).

[38] A. Nelson and C. Prescod-Weinstein, *Relaxion: A Landscape Without Anthropic*, *Phys. Rev.* **D96** (2017) 113007, [[1708.00010](#)].

[39] K. S. Jeong and C. S. Shin, *Peccei-Quinn Relaxion*, *JHEP* **01** (2018) 121, [[1709.10025](#)].

[40] T. You, *A Dynamical Weak Scale from Inflation*, *JCAP* **1709** (2017) 019, [[1701.09167](#)].

[41] M. Son, F. Ye and T. You, *Leptogenesis in Cosmological Relaxation with Particle Production*, [1804.06599](#).

[42] A. Kusenko, K. Schmitz and T. T. Yanagida, *Leptogenesis via Axion Oscillations after Inflation*, *Phys. Rev. Lett.* **115** (2015) 011302, [[1412.2043](#)].

[43] D. Jiménez, K. Kamada, K. Schmitz and X.-J. Xu, *Baryon asymmetry and gravitational waves from pseudoscalar inflation*, *JCAP* **1712** (2017) 011, [[1707.07943](#)].

[44] L. Kofman, A. D. Linde, X. Liu, A. Maloney, L. McAllister and E. Silverstein, *Beauty is attractive: Moduli trapping at enhanced symmetry points*, *JHEP* **05** (2004) 030, [[hep-th/0403001](#)].

[45] D. Green, B. Horn, L. Senatore and E. Silverstein, *Trapped Inflation*, *Phys. Rev.* **D80** (2009) 063533, [[0902.1006](#)].

[46] L. Pearce, M. Peloso and L. Sorbo, *The phenomenology of trapped inflation*, *JCAP* **1611** (2016) 058, [[1603.08021](#)].

[47] M. M. Anber and L. Sorbo, *Naturally inflating on steep potentials through electromagnetic dissipation*, *Phys. Rev.* **D81** (2010) 043534, [[0908.4089](#)].

[48] J. C. Pati and A. Salam, *Lepton Number as the Fourth Color*, *Phys. Rev.* **D10** (1974) 275–289.

[49] R. N. Mohapatra and J. C. Pati, *A Natural Left-Right Symmetry*, *Phys. Rev.* **D11** (1975) 2558.

[50] R. N. Mohapatra and J. C. Pati, *Left-Right Gauge Symmetry and an Isoconjugate Model of CP Violation*, *Phys. Rev.* **D11** (1975) 566–571.

[51] G. Senjanovic and R. N. Mohapatra, *Exact Left-Right Symmetry and Spontaneous Violation of Parity*, *Phys. Rev.* **D12** (1975) 1502.

[52] G. Cacciapaglia and F. Sannino, *Fundamental Composite (Goldstone) Higgs Dynamics*, *JHEP* **04** (2014) 111, [[1402.0233](#)].

[53] B. Gripaios, M. Nardecchia and T. You, *On the Structure of Anomalous Composite Higgs Models*, *Eur. Phys. J.* **C77** (2017) 28, [[1605.09647](#)].

[54] E. Molinaro, F. Sannino, A. E. Thomsen and N. Vignaroli, *Uncovering new strong dynamics via topological interactions at the 100 TeV collider*, *Phys. Rev.* **D96** (2017) 075040, [[1706.04037](#)].

[55] M. Chala, G. Durieux, C. Grojean, L. de Lima and O. Matsedonskyi, *Minimally extended SILH*, *JHEP* **06** (2017) 088, [[1703.10624](#)].

[56] PARTICLE DATA GROUP collaboration, C. Patrignani et al., *Review of Particle Physics*, *Chin. Phys.* **C40** (2016) 100001.

[57] A. D. Linde, *Infrared Problem in Thermodynamics of the Yang-Mills Gas*, *Phys. Lett.* **96B** (1980) 289–292.

[58] D. J. Gross, R. D. Pisarski and L. G. Yaffe, *QCD and Instantons at Finite Temperature*, *Rev. Mod. Phys.* **53** (1981) 43.

[59] J. R. Espinosa, M. Quiros and F. Zwirner, *On the nature of the electroweak phase transition*, *Phys. Lett.* **B314** (1993) 206–216, [[hep-ph/9212248](#)].

[60] M. L. Bellac, *Thermal Field Theory*. Cambridge University Press, 2011.

[61] CMS collaboration, C. Collaboration, *Search for high-mass $Z\gamma$ resonances in proton-proton collisions at $\sqrt{s} = 13$ TeV*, .

[62] S. Alekhin et al., *A facility to Search for Hidden Particles at the CERN SPS: the SHiP physics case*, *Rept. Prog. Phys.* **79** (2016) 124201, [[1504.04855](#)].

[63] E. Bertuzzo, N. Fonseca, L. de Lima and E. Morgante, *work in progress*, .

[64] F. Bezrukov and D. Gorbunov, *Light inflaton Hunter's Guide*, *JHEP* **05** (2010) 010, [[0912.0390](#)].

[65] E. W. Kolb and M. S. Turner, *The Early Universe*, *Front. Phys.* **69** (1990) 1–547.

[66] D. Cadamuro and J. Redondo, *Cosmological bounds on pseudo Nambu-Goldstone bosons*, *JCAP* **1202** (2012) 032, [[1110.2895](#)].

[67] M. Kawasaki, K. Kohri, T. Moroi and Y. Takaesu, *Revisiting Big-Bang Nucleosynthesis Constraints on Long-Lived Decaying Particles*, *Phys. Rev.* **D97** (2018) 023502, [[1709.01211](#)].

[68] M. Kawasaki, K. Kohri and N. Sugiyama, *MeV scale reheating temperature and thermalization of neutrino background*, *Phys. Rev.* **D62** (2000) 023506, [[astro-ph/0002127](#)].

[69] D. J. Fixsen, E. Dwek, J. C. Mather, C. L. Bennett and R. A. Shafer, *The Spectrum of the extragalactic far infrared background from the COBE FIRAS observations*, *Astrophys. J.* **508** (1998) 123, [[astro-ph/9803021](#)].

[70] PLANCK collaboration, P. A. R. Ade et al., *Planck 2015 results. XIII. Cosmological parameters*, *Astron. Astrophys.* **594** (2016) A13, [[1502.01589](#)].

[71] H. Ishida, M. Kusakabe and H. Okada, *Effects of long-lived 10 MeV-scale sterile neutrinos on primordial elemental abundances and the effective neutrino number*, *Phys. Rev.* **D90** (2014) 083519, [[1403.5995](#)].

[72] V. Poulin and P. D. Serpico, *Nonuniversal BBN bounds on electromagnetically decaying particles*, *Phys. Rev.* **D91** (2015) 103007, [[1503.04852](#)].

[73] S. Enomoto, S. Iida, N. Maekawa and T. Matsuda, *Beauty is more attractive: particle production and moduli trapping with higher dimensional interaction*, *JHEP* **01** (2014) 141, [[1310.4751](#)].